Charles University in Prague
Faculty of Mathematics and Physics

DIPLOMA THESIS

Tomáš Kosek

Jet modification in heavy ion collisions

Institute of Particle and Nuclear Physics

Supervisor: RNDr. Jiří Dolejší, CSc.,
Study program: Physics
Study field: Nuclear and Subnuclear Physics

2009

Univerzita Karlova v Praze
Matematicko-fyzikální fakulta

DIPLOMOVÁ PRÁCE

Tomáš Kosek

Ovlivnění jetů ve srážkách těžkých iontů

Ústav částicové a jaderné fyziky

Vedoucí diplomové práce: RNDr. Jiří Dolejší, CSc.,
Studijní program: Fyzika
Studijní obor: Jaderná a subjaderná fyzika

2009

Acknowledgement I would like to thank to my supervisor Dr. Jiří Dolejší for his guidance during the creation of my diploma thesis, for consultations and number of advices he gave me. I am also grateful to Martin Spousta for his advices and ideas he gave me and for discussions over obtained results we had. I would also like to thank to Martin Rybář fo the discussions about heavy ion collisions. Last but not least I would like to thank to my family and friends which supported me during the whole duration of my studies.

Prohlašuji, že jsem svou diplomovou práci napsal(a) samostatně a výhradně s použitím citovaných pramenů. Souhlasím se zapůjčováním práce a jejím zveřejňováním.

I declare that I wrote my diploma thesis independently and exclusively with the use of the cited sources. I agree with lending the thesis.

In Prague, 16^{th} August 2009 Tomáš Kosek

Contents

Název práce: Ovlivnění jetů ve srážkách těžkých iontů
Autor: Tomáš Kosek
Katedra (ústav): Ústav částicové a jaderné fyziky
Vedoucí diplomové práce: RNDr. Jiří Dolejší, CSc.
e-mail vedoucího: dolejsi@ipnp.troja.mff.cuni.cz

Abstrakt: V předložené práci se zabýváme jevem zvaným jet quenching, zejména pak jeho implementací v simulačních programech HIJING a PYQUEN. Jet quenching je dlouho předpovězený jev, který byl experimentálně pozorován ve srážkách těžkých iontů na urychlovači RHIC a na jehož studium se také připravují experimenty na urychlovači LHC v CERNu. Některé simulační programy používané pro přípravu těchto experimentů v sobě mají mechanismu jet quenchingu v nějaké formě implementován. V této práci jsou detailně rozebrány dva modely jet quenching jak jsou implementované v programech HIJING a PYQUEN, jaké jsou volné parametry těchto modelů a jak změna těchto parametrů mění výsledek simulací.

Klíčová slova: kvark-gluonové plasma, srážky těžkých iontů, jet quenching, HIJING, PYQUEN

Title: Jet quenching in heavy ion collisions
Author: Tomáš Kosek
Department: Institue of Particle and Nuclear Physics
Supervisor: RNDr. Jiří Dolejší, CSc.
Supervisor's e-mail address: dolejsi@ipnp.troja.mff.cuni.cz

Abstract: In the present work we study the phenomenon called jet quenching, we are interested mainly in the implementation of the jet quenching in programs HIJING and PYQUEN. Jet quenching was first proposed a long time ago but was firstly observed quite recently at Relativstic Heavy Ion Collider RHIC. Experiments at the Large Hadron Collider LHC in CERN are also preparing for measurement of jet quenching. Some simulation programs used for the preparation of these experiments have jet quenching implemented in some way. In this work we discuss, how exactly are two models of jet quenching implemented in HIJING and PYQUEN programs, which free parameters models contain and how variation of these parameters changes results of the simulations.

Keywords: quark-gluon plasma, heavy ion collisions, jet quenching, HIJING, PYQUEN

Introduction

Jet quenching is one of the signatures of quark-gluon plasma (QGP) formation in heavy ion collisions. It was firstly observed at Relativistic Heavy Ion Collider in Brookhaven National Laboratory. Quark-gluon plasma is one of the phases of matter, predicted by quantum chromodynamics (QCD), a fundamental theory of strong interaction. The basic introduction into QCD and motivation why to study quark-gluon plasma is given in the first chapter.

The collisions of heavy ions is the only way, how to study possible quark-gluon plasma formation in the laboratory. The question whether QGP is formed or not in heavy ion collisions is still not definitely answered, however there are several signatures suggesting that QGP is created in heavy ion collisions. These signatures together with basic description of heavy ion collisions are discussed in the chapter 2.

One of the most promising signatures of QGP formation is phenomenon called jet quenching. The necessary condition for the jet quenching existence is that parton traversing quark-gluon plasma loses a significant amount of energy relative to parton traversing through nuclear matter. Both theoretical calculations and experimental results from RHIC are discussed in chapter 3 confirm this assumption.

The heavy ion collisions should be accessible also on the Large Hadron Collide (LHC) which, as we hope, will start its operation during the autumn of this year (2009). To prepare experiments for the various measurements the simulation programs are widely used. One of the widely used programs in heavy ion community is HIJING, which also implements the mechanism of jet quenching. In chapter 4 we analyse, how the heavy ion event is generated in HIJING, how does the jet quenching look like, how many free parameters in model are and how variation of these parameters changes some of the properties of generated event. Newer and also more sofisticated program which simulates jet quenching is PYQUEN. But in contrast to HIJING, the PYQUEN does not compute the full heavy ion event, it "only" modifies PYTHIA events (PYTHIA is a "standard simulation program for pp collisions). PYQUEN is discussed in chapter 5. Brief conclusion of our analyses and obtained results is given in chapter 6.

In this thesis the natural system of units is used: $c = 1$, $\hbar = 1$.

Chapter 1

QCD

1.1 Standard Model

The basic theoretical tool describing elementary particles interactions is the so-called Standard Model, a well established theory which describes three of four fundamental interactions. It is gauge theory with the gauge group $SU(3) \times SU(2) \times U(1)$. Interactions described by standard model are:

- *electromagnetic interaction* which acts between all electrically charged particles, i.e. protons, electrons etc. Electromagnetic force is mediated by the exchange of photons. This interaction is responsible for most of the phenomena in our everyday life except gravitational effects – for example atoms are bound states of positively charged nuclei and negatively charged electrons. Quantum field theory of electromagnetic interaction is called Quantum Electrodynamic (QED).

- *weak interaction* acts on leptons (both charged both electrically neutral) and quarks. The weak interaction carriers are W and Z bosons. Since these bosons are very heavy (80.4 resp. 91.2 GeV), weak force has very short range. Weak interaction is responsible for beta decay and the associated radioactivity. In late 60's the electroweak theory was developed – in this theory electromagnetic and weak interactions are considered as two different aspects of one electroweak interaction.

- *strong interaction* was historically discovered as the force which acts on protons and neutrons and binds them into the atomic nuclei. Hence this force was named nuclear force. Nowadays we know that strong interaction affects more fundamental particles, the so-called quarks, and that nuclear force is only residual part of the strong interaction. Force between quarks is mediated by the exchange of particles called gluons – both quarks and gluons carry the so-called colour charge which is an analogy to electrical charge known from everyday life. All colour charged particles are in normal conditions confined into the colour neutral particles, hadrons. The quantum field theory applied to strong interaction is Quantum Chromodynamics (QCD) which will be discussed in more detail in following sections.

1.2 Motivation for QCD

In 1964 in order to explain results of hadron spectroscopy, Murray Gell-Mann and independently George Zweig proposed, that hadrons are composed from more fundamental particles which Gell-Mann named quarks – the quark model (QM) was born [1]. According to quark model, quarks are spin 1/2 fermions which come in six flavours. Baryons are composed of three quarks, antibaryons are composed of three antiquarks and mesons are composed of a quark and an antiquark. Thus the baryon number of each quark is 1/3 and of each antiquark -1/3.

Quark model can successfully explain hadron static properties like mass, spin or magnetic moment. However, soon after the birth of quark model, the problem with statistics appeared, it seemed that QM violates Pauli exclusion principle. According to quark model, Δ^{++} baryon is composed of three identical u quarks in the same state – this is inconsistent with the Pauli principle. The way out of this dilemma is to impose new quantum number called colour – now quarks come not only in six flavours but also in three colours. Each quark which forms baryon is in different colour so that Pauli principle is satisfied. Another argument, that quarks exist in three colours is given in section 1.3.

If proton is composed of quarks, one might expect that proton could be hit so hardly, that it breaks down into isolated quarks. Since at least one quark should be stable one might be able to detect it. Despite more than 20 years long experimental effort, isolated quark has never been observed. This fact lead physicists to introduce the concept of *quark confinement* – quarks cannot be isolated, they are forever confined into hadrons.

In the late 1960s, experimental results from electron-proton scattering experiments performed at SLAC-MIT lead Feynman and Bjorken to formulation of the so-called *parton model* (the brief introduction into parton model is in Appendix A). In this model, proton is assumed to be a loosely bound assemblage of a small number of constituents, called partons. Partons were assumed to be point-like fermions[1] which are unable to exchange large momenta via strong interaction at high energies, however their electromagnetic interaction is unchanged and is driven by QED.

Problem of incorporating of these two at first sight contradictory properties, i. e. confinement of quarks in hadrons and "weakness" of strong interaction at high energies, into one theory was resolved by the discovery of *asymptotic freedom* in non-Abelian gauge theories and subsequent formulation of Quantum Chromodynamics.

1.3 QCD as a gauge theory

Fundamental question in construction of gauge theory of strong interaction is how many colours are there, because number of colours determines the gauge group of the strong interaction. One of the verifications, that there are three colours is the ratio of the cross

[1]Nowadays also gluons are considered as partons, so this statement is not correct anymore – gluons are bosons and do not interact via electromagnetic interaction

section for hadronic and muonic reactions in e^+e^- pair annihilation. This ratio is given by

$$R = \frac{\sigma(e^+e^- \to \text{hadrons})}{\sigma(e^+e^- \to \mu^+\mu^-)} = \left(\sum_q Q_q^2\right) N_c \tag{1.1}$$

where N_c is the number of colours. This relation is in agreement with experiment if $N_c = 3$. Thus, in analogy with electroweak theory, we can regard quarks as the fundamental representation of a SU(3) colour group. Then the four-potential and "gauge angle" can be written as [2]

$$\hat{A}_\nu(x) = \sum_{a=1}^{8} \frac{1}{2}\hat{\lambda}_a A_\nu^a(x) \tag{1.2}$$

$$\hat{\theta}(x) = \sum_{a=1}^{8} \frac{1}{2}\hat{\lambda}_a \theta^a(x) \tag{1.3}$$

where $\hat{\lambda}_a$ are SU(3) (also called Gell-Mann) matrices. Corresponding gauge transformations are

$$\hat{A}_\nu(x) \to \hat{A'}_\nu(x) = e^{ig\hat{\theta}(x)}\left(\hat{A}_\nu(x) + \frac{i}{g}\partial_\nu\right)e^{-ig\hat{\theta}(x)}, \tag{1.4}$$

$$\Psi(x) \to \Psi'(x) = e^{ig\hat{\theta}(x)}\Psi(x) \tag{1.5}$$

where $\Psi(x)$ is the quark wave function which now is colour-SU(3) triplet

$$\Psi(x) = \begin{pmatrix} \Psi_r(x) \\ \Psi_b(x) \\ \Psi_g(x) \end{pmatrix} \tag{1.6}$$

and the Lagrangian is

$$\mathcal{L} = -\frac{1}{2}\text{tr}(\hat{F}_{\mu\nu}\hat{F}^{\mu\nu}) + \bar{\Psi}(p_\mu + g\hat{A}_\mu)\gamma^\mu\Psi \tag{1.7}$$

with the tensor of the gluon field strength

$$\hat{F}_{\mu\nu} = (\partial_\mu A_\nu^a - \partial_\nu A_\mu^a + g f^{abc} A_\mu^b A_\nu^c)\frac{\lambda^a}{2} \tag{1.8}$$

where f^{abc} is the structure constant of the SU(3) symmetry group.

1.4 Asymptotic freedom, pQCD

In section 1.2 we indicated that asymptotic freedom played an important role in formulation of QCD as a non-Abelian gauge theory. Moreover it is important property of QCD since it ensures the possibility to use perturbation expansion to calculate strong

interaction processes at high energies and thus it provides possibility to compare QCD predictions with experiment. It was discovered in 1973 by David Gross and Frank Wilczek and independently of them by David Politzer.

To prove that QCD is asymptotically free theory, one has to compute the so-called beta-function. By this function dependence of the coupling parameter g on the energy scale μ is governed [3]

$$\mu \frac{\mathrm{d}g(\mu)}{\mathrm{d}\mu} = \beta(g(\mu)). \tag{1.9}$$

g is related to coupling constant α_s by relation $\alpha_s(\mu^2) = g^2(\mu)/4\pi$. The beta function is a power series in g

$$\beta(g) = -g\left(\frac{\alpha_s}{4\pi}\beta_1 + \left(\frac{\alpha_s}{4\pi}\right)^2 \beta_2 + \ldots\right) \tag{1.10}$$

In QCD, β_1 is

$$\beta_1 = (11N_c - 2n_f)/3 \tag{1.11}$$

where N_c is number of colours and n_f is number of quark flavours. We can see that β is positive for $n_f \leq 16$. The coupling constant α_s then can be written (in the lowest order) as

$$\alpha_s(\mu^2) = \frac{\alpha_s(\mu_0^2)}{1 + (\beta_1/4\pi)\alpha_s(\mu_0^2)\ln(\mu^2/\mu_0^2)} \tag{1.12}$$

It is convenient to write α_s as

$$\alpha_s(\mu^2) = \frac{4\pi}{\beta_1 \ln(\mu^2/\Lambda_{\mathrm{QCD}}^2)} \tag{1.13}$$

where

$$\Lambda_{\mathrm{QCD}} = \mu_0 e^{-2\pi/(\beta_1 \alpha_s(\mu_0^2))} \tag{1.14}$$

is the QCD scale. It's measured value is ≈ 200 MeV. Behaviour of α_s as a function of $\mu = \sqrt{\mu^2}$ is depicted in figure 1.1

As we now know, QCD coupling constant becomes small as the momentum transfer is large enough. This ensures, that perturbation expansion can be used. "Smallness" of the coupling constant is necessary condition for usage of perturbation expansion. If the coupling constant isn't small enough, the problems with perturbative expansion convergence arose. The theory which applies perturbation theory to strong interaction processes is called perturbative QCD (pQCD) – the threshold for usage pQCD is when $Q \approx 1$ GeV. Then $\alpha_s(Q_c) \approx 0.4$ (see equation 1.13). For $Q \geq Q_c$ the well known Feynman rules may be used for calculation of the S matrix elements. The differential cross section for parton-parton scattering then is

$$\frac{\mathrm{d}\sigma}{\mathrm{d}t} = \frac{\pi\alpha_s^2}{s^2}\overline{|\mathcal{M}|^2} \tag{1.15}$$

where corresponding matrix elements $\overline{|\mathcal{M}|^2}$ are listed in Appendix B.

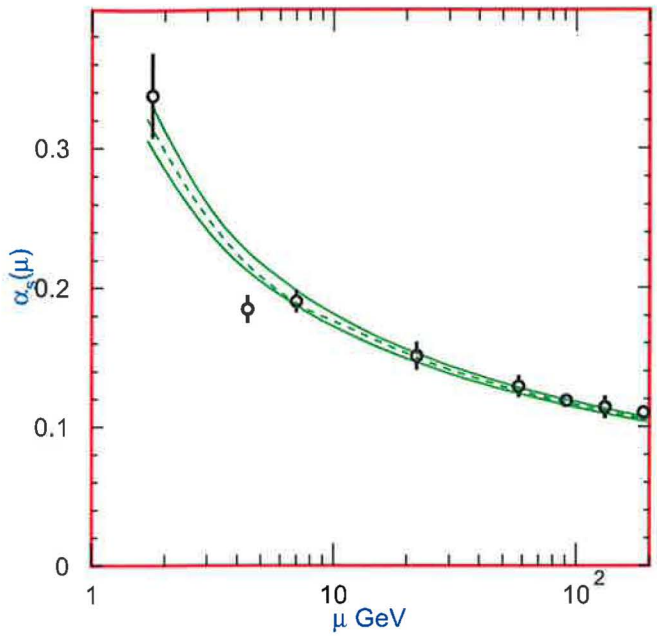

Figure 1.1: α_s dependence on μ. Taken from [4]

1.5 Fragmentation

When two partons undergo scattering they can be kicked out of the parent hadrons. But as we know, partons are confined into hadrons – the bridge between "parton world" and "hadron world" is provided by process called fragmentation (or equivalently hadronization). This process is not yet fully understood so one has to rely on phenomenological models which well describe fragmentation but contain free parameters which cannot be estimated from the theory (QCD). One of these models is Lund string model which will be discussed a bit further.

The bound state of quark-antiquark pairs (i. e. mesons) can be described by the inter-quark potential V of the form [1]

$$V(r) = -\frac{4}{3}\frac{\alpha_s}{r} + \kappa r \tag{1.16}$$

where the first part is important at short distances whereas the second describes the phenomenon of confinement. κ is the strength of the colour electric force acting on a colour charge. Now as r increases, the second term in 1.16 takes over so that $q\bar{q}$ potential rises linearly with separation. The lines of chromo-electric flux between quark and an antiquark are depicted in figure 1.2. In the case of an infinitely thin colour flux-tube κ corresponds to the tension in the stringlike force field. To produce the massive (mass μ) quark-antiquark pair the field energy in between must be sufficient. This gives the condition to the distance l_{min}

$$2\kappa l_{min} = 2\mu \tag{1.17}$$

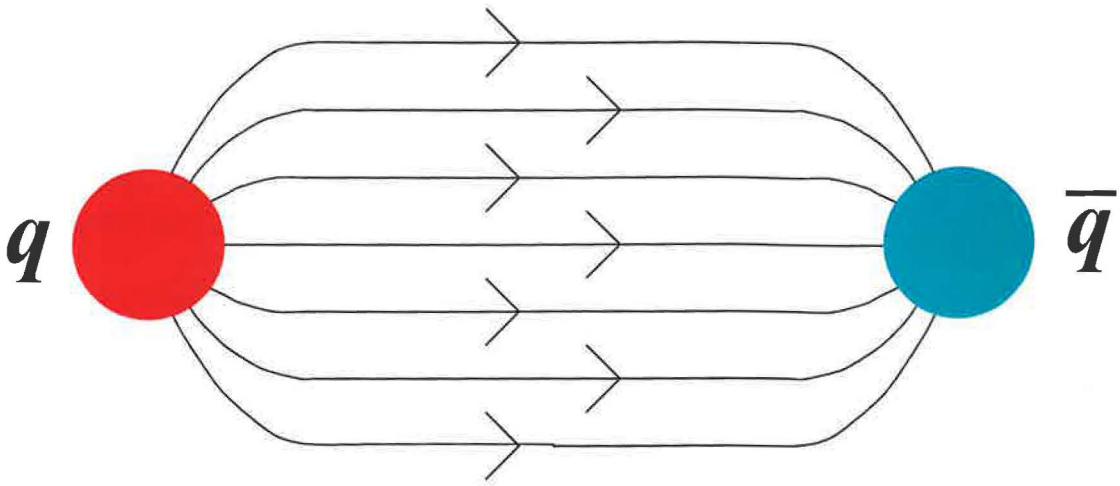

Figure 1.2: Chromo-electric field between quark and an antiquark, the so called flux-tube. Taken from [6]

The production of the quark-antiquark pair may be considered as a tunnelling process in a linear potential. The production matrix element is the overlap between the initial field and the final state particle-antiparticle wavefunction and in the simplest calculation holds [5]

$$|\mathcal{M}|^2 \approx \exp - \left(\frac{\pi \mu_\perp^2}{\kappa} \right) \tag{1.18}$$

where $\mu_\perp = \sqrt{\mu^2 + p_\perp^2}$ is the transverse mass. This is the basic result for the tunnelling process. There are more precise calculation taking into account finite size field corrections, but the result 1.18 will be the same. This formula also gives the suppression of heavier quark pairs production

$$u : d : s : c \simeq 1 : 1 : \frac{1}{3} : 10^{-11} \tag{1.19}$$

1.6 Jets

Jet is a narrow cone of hadrons produced in hard scattering of leptons, hadrons or gauge bosons. In any case, to produce jet, the hard parton has to be produced in the scattering of incident particles. As we know from previous section, such partons hadronize before they can be detected into the spray of hadrons which is called jet. The typical event with two jets produced is in figure 1.3. We will now discuss a case of two hadrons collision in the center of mass frame (CMS)

Let's have a collision of proton with four-momentum P_1 with proton with four-momentum P_2. In this collision two elementary particles 3 and 4 with four-momentum p_3 and p_4 plus some remnant system of particles (X) are produced . The the Mandelstam

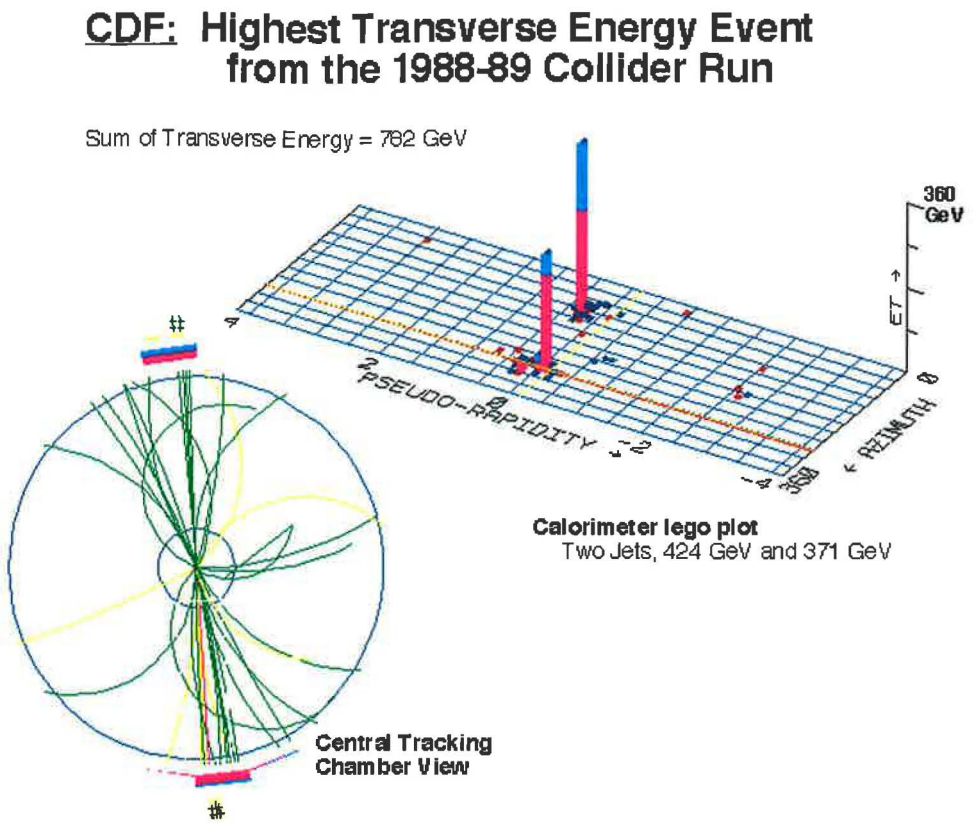

Figure 1.3: The event with two high E_{T} jets as seen in the CDF experiment in Fermilab. Taken from [7]

variables usually used for scattering process description have the following form

$$s = (P_1 + P_2)^2 \tag{1.20}$$

$$t = (p_3 - P_1)^2 \tag{1.21}$$

$$u = (p_3 - P_2)^2 \tag{1.22}$$

Protons are composed of partons with momentum $p_{1,2}$ which carry part $x_{1,2}$ of the proton momentum $P_{1,2}$. This can be expressed by relation

$$p_1 = x_1 P_1, \qquad p_2 = x_2 P_2 \tag{1.23}$$

Neglecting masses, the Mandelstam variables at the parton level then can be written as

$$\hat{s} = (p_1 + p_2)^2 = x_1 x_2 s \tag{1.24}$$

$$\hat{t} = (p_3 - p_1)^2 = x_1 t \tag{1.25}$$

$$\hat{u} = (p_3 - p_2)^2 = x_2 u \tag{1.26}$$

Probability, that parton of type f carries fraction x of the proton momentum is expressed by the parton distribution function $f_f(x)$ (see Appendix A). It is now straightforward to write the cross section for process $pp \to 3 + 4 + X$ in parton variables

$$\frac{\mathrm{d}^3\sigma}{\mathrm{d}x_1\,\mathrm{d}x_2\,\mathrm{d}\hat{t}}(pp \to 3 + 4 + X) = f_1(x_1)f_2(x_2)\frac{\mathrm{d}\sigma}{\mathrm{d}\hat{t}}(1 + 2 \to 3 + 4) \tag{1.27}$$

where differential cross section $\mathrm{d}\sigma/\mathrm{d}\hat{t}$ can be obtained from relation 1.15. The relation 1.27 can be translated into observable parameters of the final state, so one can get [8]

$$\frac{\mathrm{d}^4\sigma}{\mathrm{d}y_3\,\mathrm{d}y_4\,\mathrm{d}^2p_\mathrm{T}}(pp \to 3 + 4 + X) = x_1f_1(x_1)x_2f_2(x_2)\frac{1}{\pi}\frac{\mathrm{d}\sigma}{\mathrm{d}\hat{t}}(1 + 2 \to 3 + 4) \tag{1.28}$$

where y_3, y_4 are the rapidities of the final-state partons.

1.7 Quark Gluon Plasma

The usually studied systems in physics are those consisting of one, two or infinite number of particles. The dynamics of few particle systems is often complicated – consider for example three body system in classical mechanics. In QCD, two particle systems at high energies are studied via perturbation theory (pQCD). However, it is also interesting to study properties of strongly interacting infinite particle systems since their properties may reflect symmetries of the QCD interactions.

As was already mentioned, hadrons are composed from quarks and gluons. At low temperature and density, hadronic matter can be described as weakly interacting gas of nucleons and pions. If temperature and density is increased, hadrons start to overlap and partonic degrees of freedom become important, quarks and gluons become free, i. e. unconfined (see figure 1.4). This phase of matter is called quark or QCD matter or quark gluon plasma (QGP) in analogy to "classical" plasma where electrons are free rather than bound into atoms. Quark matter exists, or existed, in several cases in the universe [9].

Cores of the relatively cold neutron stars are compressed by its own weight to extremely high (baryon) density, such high that it is reasonable to expect, that quark matter exists there. Since neutron stars has macroscopic lifetimes, and since the time scale for strongly interacting systems is 10^{-23} s, this form of QCD matter is in thermal equilibrium. The fact if phase of matter is in thermal equilibrium or not is very important since it determines whether or not equilibrium thermodynamic may be used.

Another system of strongly interacting matter was provided by big bang. It is expected, that shortly after the big bang, in the time of the order 10^{-5} s, the whole universe was in the form of the quark gluon plasma. Once again, since 10^{-5} s is very long time relative to strong interaction time scale, the Universe was probably in local thermal equilibrium.

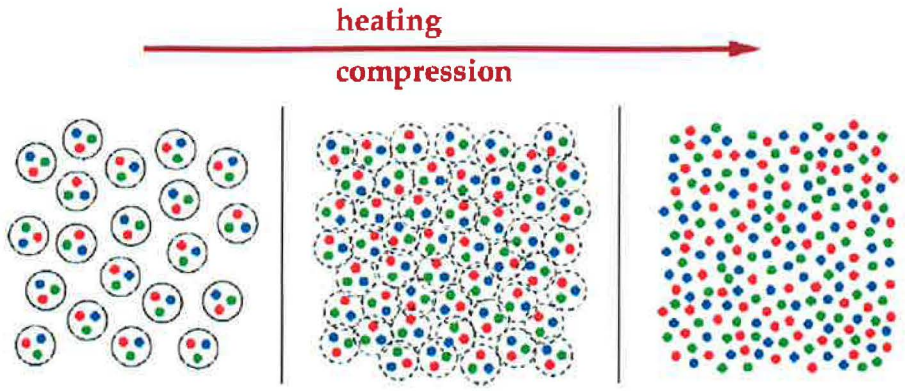

Figure 1.4: Illustration of transition between hadronic matter and QGP. Taken from [10]

The only way to produce very hot and dense matter which could be directly studied in the laboratory is to collide heavy ions in the colliders. The question whether QGP is produced or not is still not definitely answered, however there are strongly suggesting experimental facts, that this really occurs. The same holds for the question on thermal equilibration – widely accepted opinion is that produced matter reaches thermal equilibration but the definite answer is missing. Heavy ion collisions will be discussed in more detail in next chapter.

We will now focus on the question, what is the temperature when partonic degrees of freedom start to play dominant role, i. e. what is the temperature at which phase transition between hadronic and partonic matter occurs. If one imagine pion gas at temperature $T \gtrsim 100$ MeV, than pion rest mass can be neglected and the pressure of the pion gas is given by the formula for blackbody radiation pressure

$$p_\pi = 3 \times \left(\frac{\pi^2}{90}\right) T^4 \tag{1.29}$$

where the factor 3 is counting for three pion charge states. Analogic formula for quark and gluon plasma with two light (massless) quark flavours and massless gluons looks as follows

$$p_{QGP} = (\overbrace{2 \times 2 \times 3 \times \frac{7}{4}}^{q-\bar{q}} + \overbrace{2 \times 8}^{g}) \left(\frac{\pi^2}{90}\right) T^4 \tag{1.30}$$

where numerical factors in first brackets gives the number of degrees of freedom: for $q - \bar{q}$ there exist 2 helicity states, 2 flavour states and 3 colour states, the factor $\frac{7}{4}$ accounts for the difference between Bose-Einstein and Fermi-Dirac statistics; for gluons (g) there are 2 helicity states and 8 colour states. It is natural to expect, that critical (transition) temperature is when pion gas and QGP are in equilibrium, in other words when the pressures are equal. However, we must take into account the confinement,

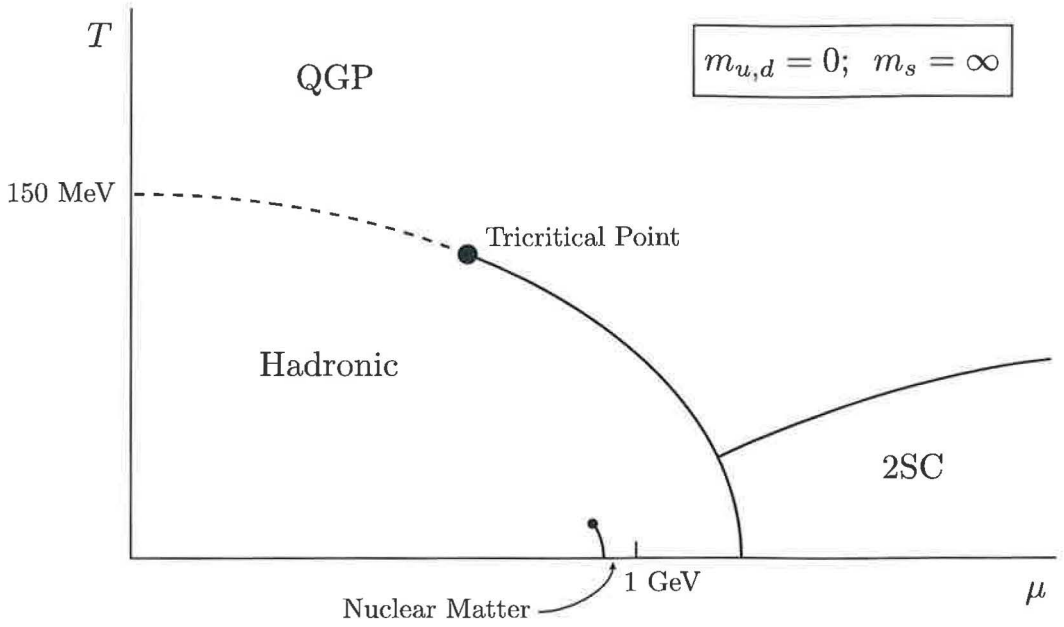

Figure 1.5: Phase diagram of nuclear matter for two massless quarks as a function of temperature T and baryon chemical potential μ. Taken from [13]

which can be characterised by the bag constant Λ_B. Value of the bag constant can be estimated from the mass of the proton, and it is approximately $\Lambda_B \sim 200$ MeV. The relation for the critical temperature than can be written as

$$\frac{3}{90}\pi^2 T_c^4 = \frac{37}{90}\pi^2 T_c^4 - \Lambda_B^4 \tag{1.31}$$

and the critical temperature is

$$T_c = \frac{\Lambda_B}{\left(\frac{34}{90}\pi^2\right)^{\frac{1}{4}}} \simeq 144 \text{ MeV} \tag{1.32}$$

The estimation we have made is crude but the obtained critical temperature is at least qualitatively correct. Experiments performed at the RHIC (Relativistic Heavy Ion Collider) estimated the critical temperature to be $T_c \simeq 175$ MeV [11]. Another way to calculate T_c is by lattice QCD (lQCD) methods. Recent result obtained from lQCD is that transition temperature is between 180 and 200 MeV [12]. For illustration, the QCD phase diagram is depicted in figure 1.5

Chapter 2

Heavy ion collisions

2.1 Space-time evolution

Existence of QGP in heavy-ion collisions is critically determined by energy density ϵ achieved in the collision. To estimate this value and also to determine whether the produced matter is in thermal equilibrium or not, one has to know how does collision looks like – what are the initial conditions and how does the system evolve in time. Despite the fact, that the picture of space-time evolution is not completely clear, the widely accepted model is that proposed by Bjorken [14]. In this model, relativistically contracted nuclei are approaching one another, each at almost speed of light. As they begin to overlap (in the z direction), each nucleon in overlapping zone (in $x - y$ plane) may undergo several collisions with nucleons in opposite nucleus loosing significant amount of energy. At this time, hard scattering also occurs and hard partons are produced. However if the energy of the nucleon is sufficient ($\sqrt{s_{NN}} \gtrsim 100$ GeV, this is satisfied for RHIC and LHC), nucleons may interpenetrate so that two receding pancakes contain the initial baryon number of the initial projectiles. The baryon free region between two pancakes is often called fireball – it is not clear what is the fireball composed from until the equilibrium is achieved. The time necessary to equilibration is predicted to be $\tau_0 = 1$ fm. Energy density in time τ_0 can be estimated by relation

$$\epsilon(\tau_0) = \frac{1}{\tau_0 \mathcal{A}} \frac{\mathrm{d}E_T}{\mathrm{d}y}\bigg|_{y=0} \tag{2.1}$$

where $\mathcal{A}$ is the nuclear overlapping area.

After the equilibrium is reached, the quark-gluon plasma might be formed. Since the thermal equilibrium is reached, the Landau hydrodynamical model can be applied. We may define a local energy density $\epsilon(x)$, pressure $p(x)$, temperature $T(x)$ and four-velocity of the fluid $u_\mu(x)$. Then the energy momentum tensor is defined as

$$T_{\mu\nu} = (\epsilon + p)u_\mu u_\nu - g_{\mu\nu}p \tag{2.2}$$

is conserved under the requirement for the momentum and energy conservation:

$$\frac{\partial T_{\mu\nu}}{\partial x_\mu} = 0 \tag{2.3}$$

Assuming only longitudinal expansion, the time dependence of the energy density is

$$\frac{\mathrm{d}\epsilon}{\mathrm{d}\tau} = -\frac{(\epsilon + p)}{\tau} \tag{2.4}$$

where τ is the proper time

$$\tau = \sqrt{t^2 - z^2} \tag{2.5}$$

As the system evolves in time, it cools down until the critical temperature is reached at time τ_c. At this time the phase transition between QGP and hadronic gas occurs. Quarks recombine and the colourless hadrons are formed. However, since the transition takes some time, the mixed phase exists until all coloured particles are bounded into hadrons. Then the interacting hadronic gas is formed, but as the system is expanding and cooling the interactions between hadrons cease and the final hadron distribution freezes out. The time evolution of the heavy ion collision can be represented by the space-time diagram – see figure 2.1.

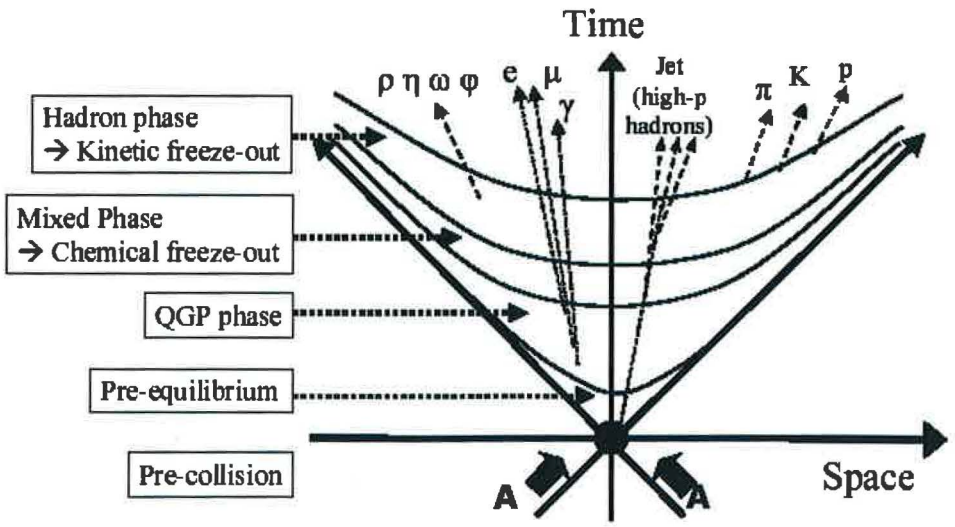

Figure 2.1: Space-time diagram of heavy ion collision. Taken from [15]

2.2 Glauber geometry

Glauber model is a standard tool for description of nucleus-nucleus collision [16]. In Glauber model, collision of two nuclei is viewed as an incoherent superposition of nucleon-nucleon interactions. The nuclei are characterised by the nuclear density which is usually considered as the Wood-Saxon's one:

$$\rho(r) = \frac{\rho_0}{1 + \exp\frac{r-R_A}{d}} \tag{2.6}$$

where $R_A \approx A^{-1/3}$ and $d \approx 0.5$ fm. Then nucleon from nucleus B (B is the mass number) hitting nucleus A at impact impact parameter $\mathbf{b}_A$ sees from nucleus A the slab of nuclear matter

$$T_A(\mathbf{b}_A) = \int_{-\infty}^{\infty} \rho(\mathbf{b}_A, z)\, \mathrm{d}z. \tag{2.7}$$

This quantity is called nuclear thickness function and is usually normalised to unity

$$\int_{-\infty}^{\infty} T_A(\mathbf{b}_A)\, \mathrm{d}\mathbf{b}_A = 1. \tag{2.8}$$

In analogy to 2.7 the baryon thickness function may be established. Then $\sigma_{in}^{NN} t(\mathbf{b})\, \mathrm{d}\mathbf{b}$ expresses the probability of inelastic nucleon-nucleon collision within the transverse element $\mathrm{d}\mathbf{b}$. The natural extension of the formula 2.7 to nucleus-nucleus collision at impact parameter $\mathbf{b}$ is to define the nuclear overlap function

$$T_{AB}(\mathbf{b}) = \int_{-\infty}^{\infty}\int_{-\infty}^{\infty} T_A(\mathbf{b}_A) T_B(\mathbf{b}_B) t(\mathbf{b} - \mathbf{b}_A - \mathbf{b}_B)\, \mathrm{d}\mathbf{b}_A\, \mathrm{d}\mathbf{b}_B. \tag{2.9}$$

Then the probability for inelastic nucleon-nucleon collision in nucleus-nucleus collision is $T_{AB}\sigma_{in}^{NN}$. If we neglect the structure of nucleon we should replace the baryon thickness function $t(\mathbf{b})$ by delta function and equation 2.9 can be simplified to

$$T_{AB}(\mathbf{b}) = \int_{-\infty}^{\infty} T_A(\mathbf{b}') T_B(\mathbf{b} - \mathbf{b}')\, \mathrm{d}\mathbf{b}. \tag{2.10}$$

Having defined the overlap function $T_{AB}(\mathbf{b})$ then the probability for the occurrence of n inelastic baryon-baryon collisions at impact parameter $\mathbf{b}$ is given by

$$P(n, \mathbf{b}) = \binom{AB}{n} [T_{AB}(\mathbf{b})\sigma_{in}]^n [1 - T_{AB}(\mathbf{b})\sigma_{in}]^{AB-n} \tag{2.11}$$

The total probability for the occurrence of an inelastic event in the AB collision at impact parameter $\mathbf{b}$ is the sum of the probabilities 2.11 from $n = 1$ to $n = AB$

$$\frac{\mathrm{d}\sigma_{in}^{AB}}{\mathrm{d}\mathbf{b}} = \sum_{n=1}^{AB} P(n, \mathbf{b}) = \sum_{n=0}^{AB} P(n, \mathbf{b}) - P(0, \mathbf{b}) = 1 - [1 - T_{AB}(\mathbf{b})\sigma_{in}]^{AB} \tag{2.12}$$

Then the total inelastic cross section σ_{in}^{AB} is

$$\sigma_{in}^{AB} = \int_{-\infty}^{\infty} \{1 - [1 - T_{AB}(\mathbf{b})\sigma_{in}]^{AB}\}\, \mathrm{d}\mathbf{b} \tag{2.13}$$

For the collision of hadron with heavy nucleus, i. e. if $B = 1$, $A \gg 1$ the total inelastic cross section is

$$\sigma_{in}^{hA} = \int_{-\infty}^{\infty} \{1 - \exp\left(-AT_{AB}(\mathbf{b})\sigma_{in}\right)\}\, \mathrm{d}\mathbf{b} \tag{2.14}$$

With the use of equation 2.11 one can derive the average number of baryon-baryon collisions in the nucleus A at impact parameter $\mathbf{b}$

$$\bar{n}(\mathbf{b}) = \frac{\sum_{n=1}^{AB} nP(n,\mathbf{b})}{\sum_{n=1}^{AB} P(n,\mathbf{b})} = \frac{ABT_{AB}(\mathbf{b})\sigma_{in}}{\mathrm{d}\sigma_{in}^{AB}/\mathrm{d}\mathbf{b}} \tag{2.15}$$

while the average number of baryon-baryon collisions for all possible impact parameters $\mathbf{b}$ is

$$\bar{n} = \frac{\int \bar{n}(\mathbf{b})(\,\mathrm{d}\sigma_{in}^{AB}/\mathrm{d}\mathbf{b})\,\mathrm{d}\mathbf{b}}{\int(\,\mathrm{d}\sigma_{in}^{AB}/\mathrm{d}\mathbf{b})\,\mathrm{d}\mathbf{b}} = \frac{AB\sigma_{in}}{\sigma_{in}^{AB}} \tag{2.16}$$

2.3 QGP Signatures

The question whether or not the quark gluon plasma in heavy ion collisions is produced still cannot be definitely answered. However, there are several phenomena, that suggest that QGP in heavy-ion collisions is produced. Some of these are strangeness enhancement, J/ψ suppression and elliptic flow. These phenomena will be briefly discussed in next paragraphs. Another QGP signature, the so called jet quenching, especially important for us so the whole next chapter is dedicated to it.

2.3.1 Strangeness enhancement

One of the first proposed signatures of QGP is strangeness enhancement [17]. The crucial argument that strange particle yields should be enhanced if QGP is formed in AA collisions is that strangeness producing processes should equilibrate faster in quark gluon plasma rather than in hadronic matter. In a thermally equilibrated medium the equilibration time depends on $\langle Q\rangle/T$. $\langle Q\rangle$ in strangeness producing processes in QGP

$$q\bar{q} \to s\bar{s}, \qquad gg \to s\bar{s} \tag{2.17}$$

is $\langle Q\rangle \approx 2m_s$ meanwhile producing processes in hadronic matter

$$\pi^+\pi^- \to KK \qquad \pi N \to \Lambda K \tag{2.18}$$

is $\langle Q\rangle \approx m_K$. Hence the strangeness abundance should reach chemical equilibrium significantly faster in QGP than in hadronic matter. In chemical equilibrium, the

strangeness relative to light quarks abundance depends only on mass difference and temperature, not on initial conditions. Since the strangeness abundance is zero at the beginning of the collision, the strange particle yields should be enhanced in the heavy-ion collisions if the QGP is formed. See figure 2.2. This is especially true for the multi-strange baryons such as $\bar{\Omega}$.

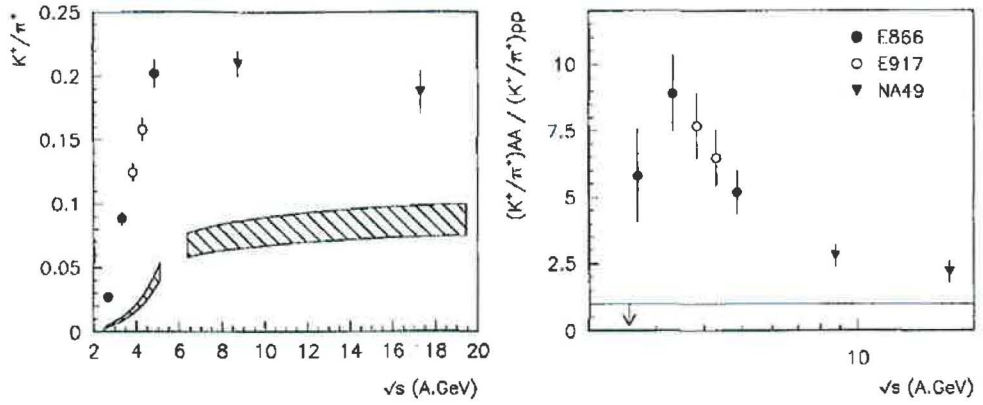

Figure 2.2: Left panel shows the measured K/π ratio from central collisions as a function of beam energy. The hashed region is the K/π ratio from pp reactions. Right panel shows the enhancement of K/π ratio. Taken from [18]

2.3.2 J/ψ suppression

J/ψ suppression in heavy-ion collisions is another proposed signature of QGP formation. J/ψ is produced in the hard scattering processes by light quark-antiquark (u, d, s) and gluon fusion: $q\bar{q}$, $gg \rightarrow c\bar{c}$. The nonrelativistic Schrödinger equation can be used for description of heavy quark-antiquark bound states with inter-quark potential [19]

$$V(r) = \kappa r - \frac{4}{3}\frac{\alpha_s}{r} \tag{2.19}$$

where first term is the confining potential with string tension κ and second is the colour Coulomb interaction. Now if we put $c\bar{c}$ pair inside the hot QCD plasma, the colour charge screening changes the inter-quark potential $V(r) \rightarrow V_{\text{eff}}(r,T)$ so that for $T > T_c$ the confining part vanishes and the second (short range) part is Debye screened and Yukawa potential arises

$$V_{\text{eff}}(r,T) \rightarrow -\frac{4}{3}\frac{\alpha_s}{r}e^{-r/\lambda_D} \tag{2.20}$$

where λ_D is the Debye screening length. Thus for $T > T_c$ inter-quark potential becomes short range and dissociation of $c\bar{c}$ can take place.

The J/ψ suppression can be explored by the ratio between J/ψ and Drell-Yan dileptons cross section. The experimental results from NA50 experiment are shown in figure 2.3.

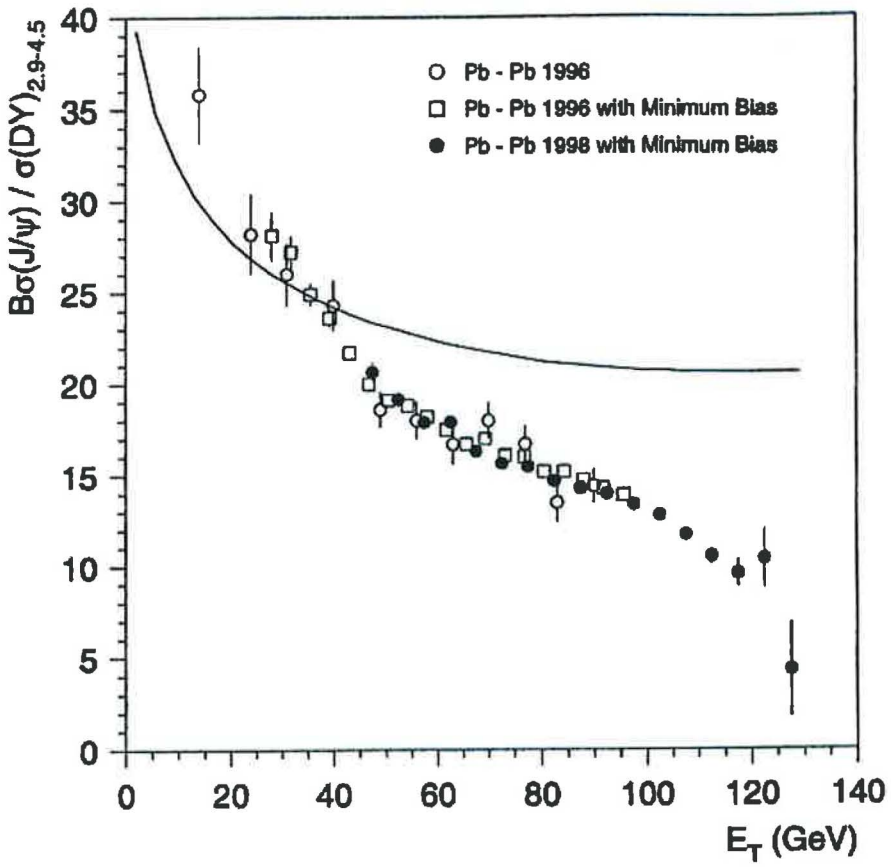

Figure 2.3: $\sigma_\psi/\sigma_{\mathrm{DY}}$ ratio as a function of E_{T}. The curve represents the J/ψ suppression due to ordinary nuclear absorption. Taken from [20]

2.3.3 Elliptic flow

The last QGP signature we will mention here is the elliptic flow [21]. In non-central collisions the overlap region of two colliding nuclei projected into the plane perpendicular to the beam direction (**z** axis) has an almond shape with the longer axis perpendicular to the reaction plane defined by the beam direction and impact parameter **b**. This asymmetry leads to the pressure gradient which then leads to the collective flow and subsequently to the azimuthally asymmetric particle emission. This can be described

by

$$E\frac{\mathrm{d}^3N}{\mathrm{d}^3p} = \frac{1}{2\pi}\frac{\mathrm{d}^2N}{p_\mathrm{T}\,\mathrm{d}p_\mathrm{T}\,\mathrm{d}y}\left[1+\sum_{n=1}^{\infty}2v_n\cos\left(n\phi\right)\right] \tag{2.21}$$

where ϕ is the azimuthal angle with respect to the reaction plane and v_n are the Fourier harmonic coefficients. The first coefficient v_1 is called direct flow, but the most important is the second coefficient v_2 called elliptic flow. If v_2 is positive, then the emission in the reaction plane is dominant. The magnitude of v_2 and its p_T dependence allows extraction of the kinetic freeze-out temperature and the transverse flow velocity as a function of emission angle.

The distribution of v_2 versus KE_T and v_2/n_q versus KE_T/n_q for π, K, p, and ϕ mesons is shown in figure 2.4. Here KE_T is the transverse kinetic energy of the particle and n_q is the number of valence quarks (2 for mesons, 3 for baryons). The universal scaling in the right panel suggests that v_2 values are developed in the partonic phase, and the hadronic phase does not lead to their modification [22].

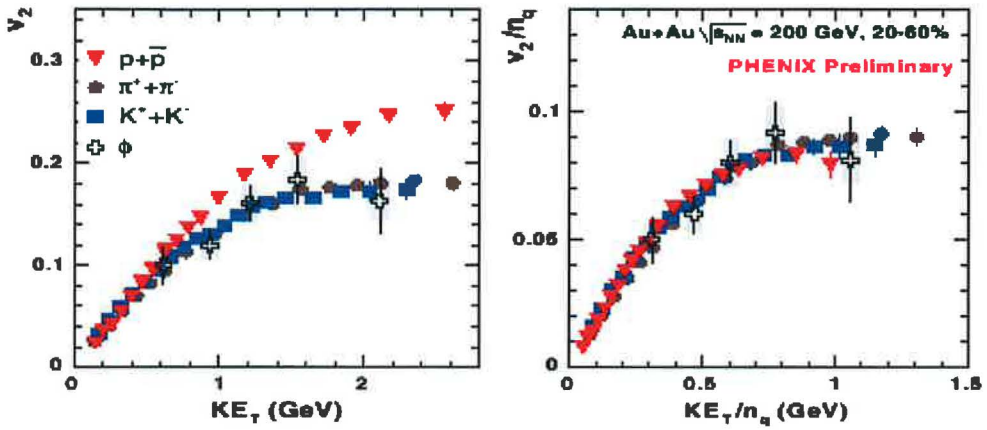

Figure 2.4: v_2 versus KE_T and v_2/n_q versus KE_T/n_q for π, K, p, and ϕ mesons detected in semi-central Au+Au collisions at $\sqrt{s_{NN}} = 200$ GeV. Taken from [22]

Chapter 3

Jet quenching

3.1 Parton energy loss

The straightforward method to obtain information about matter produced in heavy-ion collisions is to compare observables obtained in proton-proton collisions (eventually proton-nucleus) to those obtained in nucleus-nucleus collisions. Thus, it is natural to study medium induced changes in the properties of high transverse momentum particles and jets created in nucleus-nucleus collisions. Furthermore, since high p_T particles are created in the very early stage of the heavy-ion collision, in the pre-equilibrium stage, their creation is not affected by the medium – this allows them to propagate through medium after the equilibration. In this sense, high p_T particles and jets may be viewed as an external probes. Moreover, since high transverse momentum partons can be produced only in processes with large momentum transfer Q^2, their cross section may be theoretically predicted using perturbative QCD.

Parton traversing through the QCD matter can loose a significant amount of energy. There are generally two types of energy loss:

- *collisional energy loss* which is caused by the elastic scattering with the medium constituents
- *radiative energy loss* which exists due to inelastic scattering with medium when additional particles (in QCD gluons) are radiated

Both collisional and radiative energy losses depend on the mass of the propagating particle. Total energy loss thus generally depends on both medium (temperature, particle-medium interaction coupling, thickness) and particle (energy, mass, charge) properties.

The average collisional energy loss per one scattering in the medium with temperature T is [23, 24]

$$\langle \Delta E_{coll}^{1scat} \rangle \approx \frac{1}{\sigma T} \int_{m_D^2}^{t_{max}} t \frac{\mathrm{d}\sigma}{\mathrm{d}t} \, \mathrm{d}t \tag{3.1}$$

where m_D is the Debye mass which characterises the typical momentum exchanges. In QCD, the first order differential cross section is equal

$$\frac{\mathrm{d}\sigma}{\mathrm{d}t} \approx C_i \frac{4\pi\alpha_s^2(t)}{t^2} \tag{3.2}$$

where C_i is colour factor which is 9/4, 1, 4/9 for gg, gq and qq scattering, and α_s is the QCD coupling constant (see section 1.4). For given particle one can calculate the energy loss per unit length

$$-\frac{\mathrm{d}E}{\mathrm{d}l} = \frac{\langle \Delta E^{tot} \rangle}{L} \tag{3.3}$$

where for incoherent scattering $\Delta E^{tot} = N.\Delta E^{1scatt}$, $N = L/\lambda$ is the medium opacity. For $E \gg M^2/T$ one obtains (q resp. g resp. Q in lower index reflects that relation holds for light quark resp. gluon resp. heavy quark)

$$-\left.\frac{\mathrm{d}E_{coll}}{\mathrm{d}l}\right|_{q,g} = \frac{1}{4} C_R \alpha_s(ET) m_D^2 \ln\left(\frac{ET}{m_D^2}\right), \tag{3.4}$$

$$-\left.\frac{\mathrm{d}E_{coll}}{\mathrm{d}l}\right|_{Q} = -\left.\frac{\mathrm{d}E_{coll}}{\mathrm{d}l}\right|_{q,g} - \frac{2}{9} C_R \pi T^2 \left[\alpha_s(M^2)\alpha_s(ET) \ln\left(\frac{ET}{M^2}\right)\right], \tag{3.5}$$

C_R is the quark ($C_R = 4/3$) respectively gluon ($C_R = 4/3$) colour charge.

Radiative energy loss per one scattering is

$$\Delta E_{rad}^{1scatt} = \int^E \omega \frac{\mathrm{d}I_{rad}}{\mathrm{d}\omega}\,\mathrm{d}\omega, \tag{3.6}$$

or

$$\Delta E_{rad}^{1scatt} = \int^E \int^{k_{T,max}} \omega \frac{\mathrm{d}^2 I_{rad}}{\mathrm{d}\omega\,\mathrm{d}k_\perp^2}\,\mathrm{d}\omega\,\mathrm{d}k_\perp^2 \tag{3.7}$$

where $\omega\,\mathrm{d}I_{rad}/\,\mathrm{d}\omega$ and $\omega\,\mathrm{d}I_{rad}/\,\mathrm{d}\omega\,\mathrm{d}k_\perp^2$ are single resp. double bremsstrahlung spectra of radiated photons or gluons with energy ω and transverse momentum $k_\perp$.

In QCD two regimes of radiative energy loss has to be considered. First is Bethe-Heitler (BH) regime, then $L \ll \lambda$ and bremsstrahlung spectra is

$$\omega \frac{\mathrm{d}I_{rad}}{\mathrm{d}\omega} \approx \alpha_s \hat{q} \frac{L^2}{\omega} \tag{3.8}$$

which implies

$$\Delta E_{rad}^{BH} \approx \alpha_s \hat{q} L^2 \ln\left(\frac{E}{m_D^2 L}\right) \tag{3.9}$$

If $L \gg \lambda$ then the Landau-Pomeranchuk-Migdal (LPM) effect takes place. The assumption that fast parton radiates gluon at each scattering doesn't hold in the dense medium. Indeed, there is a non-zero length $l_f^{med}(\omega)$ needed for gluon formation. If now $l_f^{med} \gg \lambda$ the gluons radiation is not incoherent furthermore. As a result, the gluons

emission is suppressed. In LPM regime one has to differentiate the soft or hard gluon emission with respect to the characteristic gluonstrahlung energy $\omega_c = \frac{1}{2}\hat{q}L^2$. Then

$$\omega \frac{\mathrm{d}I_{rad}}{\mathrm{d}\omega} \approx \alpha_s \sqrt{\hat{q}L^2/\omega} \tag{3.10}$$

$$\Delta E_{rad}^{LPM} \approx \alpha_s \hat{q} L^2 \tag{3.11}$$

for $\omega < \omega_c$, and

$$\omega \frac{\mathrm{d}I_{rad}}{\mathrm{d}\omega} \approx \alpha_s \hat{q} L^2/\omega \tag{3.12}$$

$$\Delta E_{rad}^{LPM} \approx \alpha_s \hat{q} L^2 \ln\left(\frac{E}{\hat{q}L^2}\right) \tag{3.13}$$

for $\omega > \omega_c$

Since these formulas were deduced only for idealised situation with an infinite-energy parton traversing through static and uniform QGP, several models describing real situation were developed. Since the detailed discussion of this models is out of the scope of this work, we present only the list of them:

- Path-integral approach to the opacity expansion (BDMPS-LCPI/ASW)
- Reaction Operator approach to the opacity expansion (DGLV)
- Higher Twist (HT)
- Finite temperature field theory approach (AMY)

3.2 RHIC experimental results

The energy loss and corresponding gluon emission have three major phenomenological consequences

- suppression of high-p_{T} hadrons
- unbalanced back-to-back high-p_{T} dihadron azimuthal correlations
- modified jet spectra, jet shapes, and fragmentation functions

The first two phenomena were measured at RHIC and the brief review of the experimental results are in following subsections

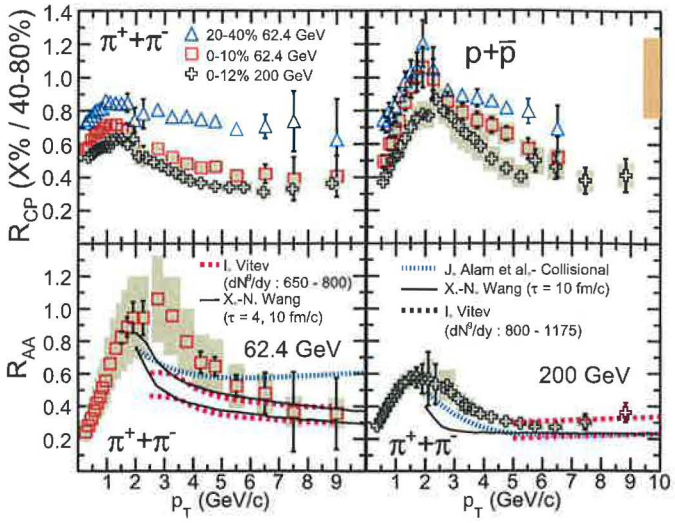

Figure 3.1: Upper panels: R_{CP} dependence on centrality (only at $\sqrt{s_{NN}} = 62.4$ GeV) and p_T for $\pi^+ + \pi^-$ and p+$\bar{\text{p}}$ at $\sqrt{s_{NN}} = 62.4$ and 200 GeV. Lower panels: R_{AA} dependence for $\pi^+ + \pi^-$ on p_T for two beam energies. Three model predictions are shown. Figure taken from [25]

3.2.1 Suppression of high-p_T hadrons

The basic quantity describing suppression of high p_{T} hadrons is the *nuclear modification factor*

$$R_{AA}(p_T, y; \mathbf{b}) = \frac{\text{"real AA collision"}}{\text{"incoherent superposition of NN collisions"}} = \frac{1}{AA.T_{AA}(\mathbf{b})} \frac{\mathrm{d}^2 N_{AA}/\mathrm{d}y\mathrm{d}p_T}{\mathrm{d}^2 N_{NN}/\mathrm{d}y\mathrm{d}p_T} \tag{3.14}$$

which measures the deviation of A+A collision at impact parameter **b** from an incoherent superposition of the nucleon-nucleon collisions. In other words, if produced partons aren't influenced by the medium produced in the collision, then $R_{AA} = 1$ for all p_T. Thus, R_{AA} is the ideal measurable for studying the medium induced changes of high p_{T} spectra in heavy ion collisions.

Nuclear modification factor can be also defined relative to peripheral collisions:

$$R_{CP} = \frac{[d^2N/p_T dy dp_T/\langle N_{bin}\rangle]^{central}}{d^2N/p_T dy dp_T/\langle N_{bin}\rangle]^{peripheral}} \tag{3.15}$$

R_{AA} dependence on p_T for $\pi^+ + \pi^-$ for two beam energies ($\sqrt{s_{NN}} = 62.4$ GeV resp. $\sqrt{s_{NN}} = 200$ GeV) and different centrality ranges is in figure 3.1 in bottom panels

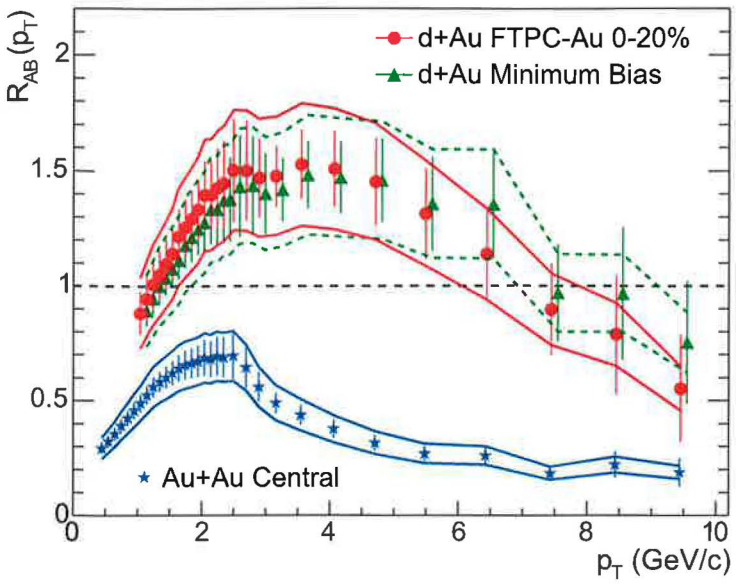

Figure 3.2: R_{dAu} dependence on p_T for minimum bias and central d+Au collisions and $R_{AA}(p_T)$ for central Au+Au collisions. Figure taken from [26]

(data are from STAR experiment, however data from all experiments at RHIC are in very good agreement). For $\sqrt{s_{NN}} = 200$ GeV, R_{AA} values are constant for $p_T \gtrsim 4$ GeV and approach value 0.2, *i. e.* the value is five time smaller than for binary-scaling expectations. In other words, strong suppression of high-p_T hadrons is observed. R_{CP} dependence on p_T, beam energy and centrality for $\pi^+\pi^-$ and p+$\bar{\text{p}}$ is in figure 3.1 in upper panels.

Figure 3.2 shows the nuclear modification factor (R_{dAu}) for minimum bias and central d+Au collisions. There is also R_{AA} for central Au+Au collisions. We can see the significant difference between R_{dAu} for d+Au and R_{AA} for Au+Au collisions: high-p_T hadrons for central Au+Au collisions are strongly suppressed by a factor ≈ 5 ($R_{AA} \approx 0.2$ for high p_T) relative to binary scaling expectations whereas in d+Au the suppression is not observed. This indicates that the suppression of high-p_T hadrons is associated with the medium produced in Au-Au collisions.

3.2.2 Dihadron azimuthal correlations

We are interested in interactions where jets are created in pairs. Then transverse momenta of jets have the same magnitude but opposite direction. If one of the mother-partons traverse significantly longer length through the hot and dense medium, the shape of the jet can be modified. This jet is called away-side jet while the jet with unchanged properties is called near-side jet. Full jet reconstruction in Au+Au collisions at RHIC is impossible due to overwhelming background of soft particles in the event. Thus, the modification of the jet shape is studied via dihadron azimuthal angle ($\Delta\phi$)

correlations.

Dihadron azimuthal angle correlations express the average number of hadrons (labelled as B) with p_T in chosen range (p_T^B) and at angular distance $\Delta\phi$ from trigger hadron A with p_T^A.

$$Y_{jet} = \frac{1}{N^A} \frac{dN^{AB}}{d\Delta\phi} \tag{3.16}$$

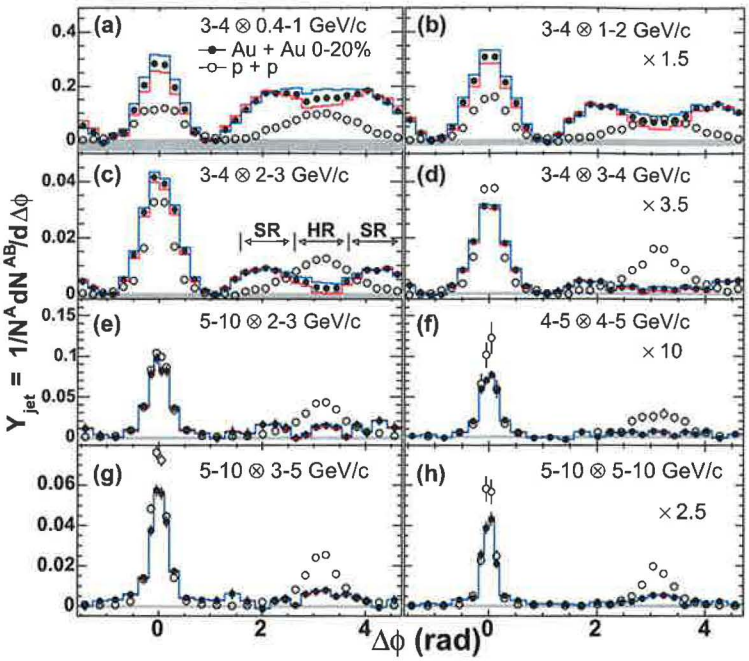

Figure 3.3: Per-trigger yields as a function of $\Delta\phi$ for various trigger and partner p_T ($p_T^A \otimes p_T^B$) in p+p and 0-20 % Au+Au collisions. Arrows in (c) indicate "head" (HR) and "shoulder" (SR) regions.

The measured per-trigger yields for p+p and 0-20 % central Au+Au at $\sqrt{s_{NN}} =$ 200 GeV are in figure 3.3. There are eight panels with different combinations of p_T^A, p_T^B ranges. The p+p data (open symbols) has Gaussian away-side peak at $\Delta\phi = \pi$ for all p_T^A and p_T^B. The Au+Au data have very different behaviour, the shape of the distribution is dependent on p_T^A and p_T^B. For a fixed value of p_T^A, panels (a)-(d) reveal a striking evolution from a broad, roughly flat peak to a local minimum at $\Delta\phi \sim \pi$ with side-peaks at $\Delta\phi \sim \pi \pm 1.1$. The location of side-peaks does not vary with increasing p_T^B and is roughly constant.

For relatively high values of $p_T^A \otimes p_T^B$ (panels (e)-(h)) the away-side jet shape for Au+Au fluently changes to Gaussian peak with similar shape as for p+p but suppressed. It seems that it is caused by bigger suppression of side-peaks at $\Delta\phi \sim \pi \pm 1.1$ relative to that at $\Delta\phi \sim \pi$.

We can see, that properties of jet, created from mother-parton which traversed through hot and dense QCD matter, are significantly changed. The away-side double-peak structure can be interpreted like medium-induced Mach-shock or Cherenkov-like gluon radiation. However, because the maximum of the side-peaks is constant with increasing p_T^B (see figure 6) it disfavours Cherenkov-like radiation.

Chapter 4

Hijing

HIJING (Heavy Ion Jet INteraction Generator) is Monte Carlo program developed in 90's to simulate full heavy ion events [27]. Authors of the program are M. Gyulassy and X.-N. Wang. HIJING is (respectively was) widely used in planning and design of heavy ion experiments at LHC (resp. RHIC) so it is important to understand in detail how it works – how is the event generated, how many parameters in the model are and consequently how variation of parameters changes generated event. HIJING is also capable to generate proton-proton and proton-nucleus collisions.

The main features of HIJING are as follows: two component formalism - soft part of the interaction is modelled via Lund-type model meanwhile hard part of the interaction is based on pQCD inspired model (Pythia). For proton-nucleus and nucleus-nucleus collisions Glauber geometry and binary approximation is used. Nuclear shadowing effect is also used to take into account. Simple scheme of jet quenching is also implemented. Some of these features and their implementation in HIJING will be discussed in more detail in next sections. We will follow the flow of the program with special emphasis focused on quenching procedure. On the other hand due to the complexity of the program some unimportant branches and details will be neglected. Also we will consider only the case when both projectile and target are nuclei.

4.1 Initialization

The latest version of the HIJING program is distributed in two files – hijing1.383.f and hipyset1.35.f. The former one contains the procedures which were written for HIJING program while the latter contains the procedures from Pythia and Jetset. The main program has to be written by user. In this program, the beam properties (collision frame, beam energy, projectile, target) are specified and passed to subroutine `HIJSET` which initialise HIJING [28]. Other input parameters for HIJING may also be specified (see for example section 4.3). The loop over events in which the procedure `HIJING` is called follows. Then the computed data should be saved.

The procedure `HIJING` is the most important part of the HIJING program which

generates complete event as specified. It is called with three parameters:

- `FRAME` which specify the frame of the collision
- `BMIN` and `BMAX` which specify the lower and upper limits (in fm) for the absolute value of the impact parameter $|\mathbf{b}| = b$. This holds only for pA and AB collisions, for hadron-hadron collisions, both values are set to zero and the events are automatically averaged over all impact parameters.

The first thing in subroutine `HIJING` is the generation of the coordinates of nucleons in nucleus according to Wood-Saxon density. The condition that two nucleons aren't closer than `HIPR1(29)` is also realized. Afterwards the impact parameter **b** is generated: $b_{\min} < b < b_{\max}$; $\varphi \in (0, 2\pi)$

4.2 Nucleon-Nucleon interaction type

After the initialization, the type of interaction between the nucleons has to be determined. For every pair of nucleons from projectile respectively target the following algorithm is repeated. First of all, the distance between nucleons is computed. Then the parameters for nuclear shadowing are determined.

Nuclear shadowing effect is one of the most important nuclear effects in relativistic heavy ion collisions. The key-stone of this effect is that parton distribution function of the nucleus is not equal to the sum of parton distribution functions of its constituents – the effective number of quarks and antiquarks is depleted in the low region of x. This is described by the ratio

$$R_A(x) = \frac{f_{a/A}(x)}{A f_{a/N}(x)}. \tag{4.1}$$

We will not go into detail with this subject, we only mention, that nuclear shadowing affects the effective jet cross section σ_{jet}^{eff}.

When the computation of nuclear shadowing parameters and effective jet cross section is finished, the differential cross section $\frac{\mathrm{d}\sigma_{tot}}{\mathrm{d}b}\big|_{b=0}$ and $\frac{\mathrm{d}\sigma_{tot}}{\mathrm{d}b}\big|_{b=b_{NN}}$ for nucleon-nucleon collision is computed. The eikonal formalism is used in HIJING [29]. If we define a real eikonal function

$$\chi(b,s) = \frac{1}{2}\sigma_{soft}(s)t(b,s) + \frac{1}{2}\sigma_{jet}(s)t(b,s) \tag{4.2}$$

where t is partonic overlap function (see section 2.2) then the elastic, inelastic and total cross sections of nucleon-nucleon collision are

$$\sigma_{\mathrm{el}} = \pi \int_0^\infty \mathrm{d}b^2 [1 - e^{-\chi(b,s)}]^2, \tag{4.3}$$

$$\sigma_{\mathrm{in}} = \pi \int_0^\infty \mathrm{d}b^2 [1 - e^{-2\chi(b,s)}], \tag{4.4}$$

$$\sigma_{\rm tot} = 2\pi \int_0^\infty {\rm d}b^2[1 - e^{-\chi(b,s)}]. \tag{4.5}$$

After the cross sections computation is done the random number $X \in \langle 0, 1\rangle$ is generated according to uniform distribution and multiplied by $\frac{{\rm d}\sigma_{tot}}{{\rm d}b}\big|_{b=0}$ so we get

$$\tilde{X} = X \left.\frac{{\rm d}\sigma_{tot}}{{\rm d}b}\right|_{b=0} \tag{4.6}$$

Now three possibilities exist

- $\tilde{X} > \frac{{\rm d}\sigma_{tot}}{{\rm d}b}\big|_{b=b_{NN}}$: then the nucleons do not interact
- $\frac{{\rm d}\sigma_{tot}}{{\rm d}b}\big|_{b=b_{NN}} > \tilde{X} > \frac{{\rm d}\sigma_{in}}{{\rm d}b}\big|_{b=b_{NN}}$: the nucleons interact only elastically. Elastic interaction is implemented in subroutine `HIJSC` which is called with two arguments `JP` and `JT` denoting nucleon's number.
- $\tilde{X} \leq \frac{{\rm d}\sigma_{in}}{{\rm d}b}\big|_{b=b_{NN}}$: the inelastic collision takes place. Then j minijets are produced with probability

  $$g_j(b) = \frac{[\sigma_{jet}^{eff} t(b)]^j}{j!} e^{-\sigma_{jet}^{eff} t(b)},\ j \geq 1 \tag{4.7}$$

  or no jet is produced with probability

  $$g_0(b) = [1 - e^{-\sigma_{soft} t(b)}] e^{-\sigma_{jet}^{eff} t(b)}. \tag{4.8}$$

  Then only soft interactions take place. Anyway, soft interactions between nucleons take place even if hard scattering occurs but with restricted kinematical conditions.

  Soft interactions are implemented in subroutine `HIJSFT` – the string phenomenology is used (combination of Lund Fritiof and Dual Parton Model). Hard scattering is managed by subsequent calls of routines `JETINI` and `HIJHRD` – in this routine, the pQCD inspired Pythia is called.

After the interactions are proceeded, the subroutine `QUENCH` (see below) is called for all nucleons and strings and at the very end the fragmentation of partons and strings is done.

4.3 Jet Quenching in HIJING

The model of jet quenching in HIJING is very simple and schematic. It is proceeded by procedure `QUENCH` which is called with two parameters `I, J` where `J` describes the kind of the object (projectile nucleon, target nucleon or string) and `I` denotes the number of the object for which the procedure is called. Despite the fact, that `QUENCH` is called for nucleons and strings, the quenched objects are partons connected with appropriate

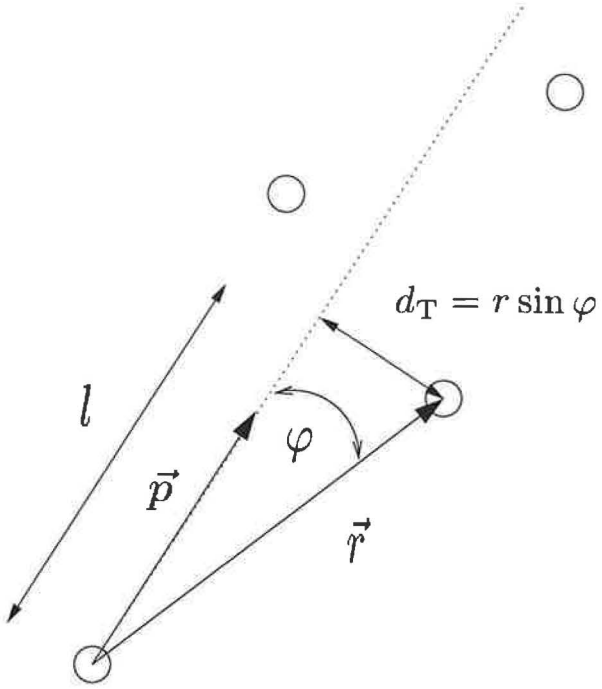

Figure 4.1: Geometry of quenching in HIJING

nucleon respectively string. Now we will describe the algorithm how the quenching is proceeded.

Quenched are only partons with $p_T > p_T^{min}$. Thus p_T^{min} is one of the parameters which affects the quenching. The p_T^{min} value can be set by `HIPR1(11)`, default value is 2 GeV. Then the objects which parton can interact with are determined:

1. it has to be excited string created in nucleon-nucleon collision
2. the absolute value of the angle φ between the direction of the partons momentum and the radius vector r has to be smaller than $\pi/2$ – see figure 4.1
3. the transverse distance $d_T = r \sin \varphi$ has to be smaller than d_T^{min} which can be set by parameter `HIPR1(12)` – this is another parameter of the HIJING quenching model, default value is 1 fm

After that, the probability of interaction is calculated

$$P = 1 - e^{-l/\lambda_s} \tag{4.9}$$

where l is depicted in the figure 4.1 and λ_s is mean free path of the parton in the excited nuclear matter. It is another free parameter of the model – the appropriate value can be set via `HIPR1(13)` and the default value is 1 fm. Then the random number X is generated according to uniform distribution and if it is bigger P, interaction with

appropriate string will not happen. Then the loop is repeated for another string. If the interaction happens, the momentum loss is proportional to the travelled length

$$\Delta p = \frac{\mathrm{d}E}{\mathrm{d}l} l. \tag{4.10}$$

where $\mathrm{d}E/\mathrm{d}l$ is the free parameter which is determined via `HIPR1(14)` with default value $\mathrm{d}E/\mathrm{d}l = 2$ GeV/fm.

Now if the quenched parton is quark, the momentum loss is one half of the gluon's loss. The new gluon is created in the place where the string is, and it's momentum is equal to the momentum lost by parton. The missing energy is taken from the string mass.

4.4 Results of simulations

We used HIJING to simulate heavy-ion collisions as will be performed at the LHC: both projectile and target are lead ions $^{208}\mathrm{Pb}^{82+}$ at $\sqrt{s_{\mathrm{NN}}} = 5500$ GeV in the centre of mass frame. We analysed only central collisions: $0 < b < 2$ fm. In every run of the program we changed one of the parameters $\mathrm{d}E/\mathrm{d}l$ or λ_s or $p_{\mathrm{T}}^{\mathrm{min}}$ (see previous section), while the remaining were set to the default values. Results of the simulations were subsequently analysed, four distributions of experimentally interesting quantities were obtained. This is in detail discussed in next four subsections.

4.4.1 Transverse energy distribution

The first distribution we will discuss is the dependence of the transverse energy E_{T} deposited into $\eta \times \phi = 0.1 \times 0.1$ bin on the pseudorapidity $-3.2 < \eta < 3.2$ – this is motivated by the granularity and coverage of the ATLAS calorimeter. The first varying parameter is $\mathrm{d}E/\mathrm{d}l$ which describes how much energy parton loses on the unit length. So with increasing $\mathrm{d}E/\mathrm{d}l$ the amount of the particle's energy loss increases. In figure 4.2 the transverse energy distribution is depicted for three values of $\mathrm{d}E/\mathrm{d}l$: 0, 2, 4 GeV/fm. We can see the increase of E_{T} in the central pseudorapidity region $-2 < \eta < 2$ by a factor ≈ 2 for events with quenching turned on. This phenomenon depends more likely on whether or not jet quenching is turned on than on the value of $\mathrm{d}E/\mathrm{d}l$.

We will get similar result, if we vary λ_s parameter. This parameter determine how many collisions parton suffers but the energy loss per unit length $\mathrm{d}E/\mathrm{d}l$ leaves unchanged. We chose values 1, 7, 10 fm. The second and third values are comparable to the diameter of the colliding nuclei, so the probability that parton suffers collision is decreased and parton might be unquenched. This exhibits in the weakening of the quenching as we can see in figure 4.3. For $\lambda_s = 1$ fm the quenching is strong and this again causes the increase of the E_{T} distribution in central pseudorapidity region, meanwhile for large values of λ_s the quenching is weak and the E_{T} distribution is modified only slightly.

The amount of the energy loss is modified also by varying of the $p_{\mathrm{T}}^{\mathrm{min}}$ which determines how many particles will be quenched and also how much energy will particle lose since particle with $p_{\mathrm{T}} = 5$ GeV can loose maximally 1 GeV for $p_{\mathrm{T}}^{\mathrm{min}} = 4$ GeV respectively 4 GeV for $p_{\mathrm{T}}^{\mathrm{min}} = 1$ GeV. So the quenching is strongly dependent on this parameter. This is clearly demonstrated in figure 4.4 where results of simulations for $p_{\mathrm{T}}^{\mathrm{min}} = 1,\ 2,\ 4$ GeV are shown. Again, if intensity of quenching increases the E_{T} increases for $-2 \lesssim \eta \lesssim 2$.

Results we just introduced are rather surprising. One would expect, that transverse energy will decrease in quenched events due to suppression of high-p_{T} partons, but our results show increase by a factor ≈ 2 in the central pseudorapidity region. The possible explanation of this contradiction is that model of jet quenching implemented in HIJING is too simple and schematic and that this model is not able to provide correct results.

4.4.2 Transverse energy per particle

Another interesting observable is the distribution of mean transverse energy per particle $\langle E_{\mathrm{T}} \rangle$. In figures 4.5-4.7 this distributions are depicted for the same sets of parameters as in previous subsection. What we can see is the opposite behaviour – the $\langle E_{\mathrm{T}} \rangle$ decreases with increasing quenching.

This is exactly what one would expect. The spectrum of the particles softens as the particles loose energy in medium. The decrease of mean transverse energy per particle is about 20 % in the central pseudorapidity region. This result seems to be quite reasonable since the decrease in mean E_{T} is significant but the behaviour of the distribution is roughly the same for quenched and non quenched events.

4.4.3 Multiplicity

As we already know from the description of the `QUENCH` procedure, also the hadron multiplicity should be changed (increased) according to gluon radiation if the quenching is proceeded. This can be quantitatively described by the distribution of multiplicity (into one bin) on the pseudorapidity. The according histograms are in figures 4.8-4.10. The multiplicity is strongly dependent namely on the $p_{\mathrm{T}}^{\mathrm{min}}$ parameter. This can be expected because the spectrum strongly decreases with p_{T} so with lower $p_{\mathrm{T}}^{\mathrm{min}}$ the number of the quenched particles and consequently the amount of radiated gluons will increase.

As we can see from figures 4.8-4.10 increase in the multiplicity is very large for events with jet quenching turned on. Increase of multiplicity can be expected according to additional gluons emitted during the interaction of parton with medium, however the factor of increase is enormous, it exceeds number 2 in figures 4.8 and 4.10. This seems to be outrageous, such big difference between quenched and non-quenched events isn't expected.

4.4.4 Relative standard deviation

In the preparation of experiments, it is important to know the detector efficiency. To determine this, it is good to know, how the fluctuations of the transverse energy deposited into the detector bin look like. We computed this as follows: we took 64 bins in ϕ at the given $\tilde{\eta}$, for every bin computed deposited transverse energy $E_{\mathrm{T}}^{\tilde{\eta},i}$ where superscript i denotes the number of bin in the ϕ direction, and then we computed standard deviation σ by

$$\sigma(\tilde{\eta}) = \sqrt{\frac{\sum_{i=1}^{64}(E_{\mathrm{T}}^{\tilde{\eta},i} - \tilde{E}_{\mathrm{T}}^{\tilde{\eta}})^2}{64}} \tag{4.11}$$

where $\tilde{E}_{\mathrm{T}}^{\tilde{\eta}}$ is the mean value of $E_{\mathrm{T}}^{\tilde{\eta},i}$ for given $\tilde{\eta}$. The histograms with $\sigma(\eta)$ distribution for three values of $\mathrm{d}E_{\mathrm{T}}/\mathrm{d}l$ is in figure 4.11. Because the multiplicity increases with increasing $\mathrm{d}E_{\mathrm{T}}/\mathrm{d}l$ one would expect that $\sigma(\eta)$ will decrease for higher values of $\mathrm{d}E_{\mathrm{T}}/\mathrm{d}l$. So the results in figure 4.11 are at first sight surprising because the σ distributions are roughly equal. This can be simply explained if we consider the increase of E_{T}. Thus the better quantity describing fluctuations is relative standard deviation

$$\delta(\eta) = \frac{\sigma(\eta)}{\tilde{E}_{\mathrm{T}}} \tag{4.12}$$

The δ distributions are depicted in figures 4.12-4.14. We can see, that relative standard deviation decreases with increasing intensity of quenching. The difference between quenched and non or weakly quenched events is about 40 %. This is indeed significant difference which can influence results of detector analysis and tests. Thus it is important to carefully consider the use of quenching procedure in HIJING since physical quantities are changed noticeably.

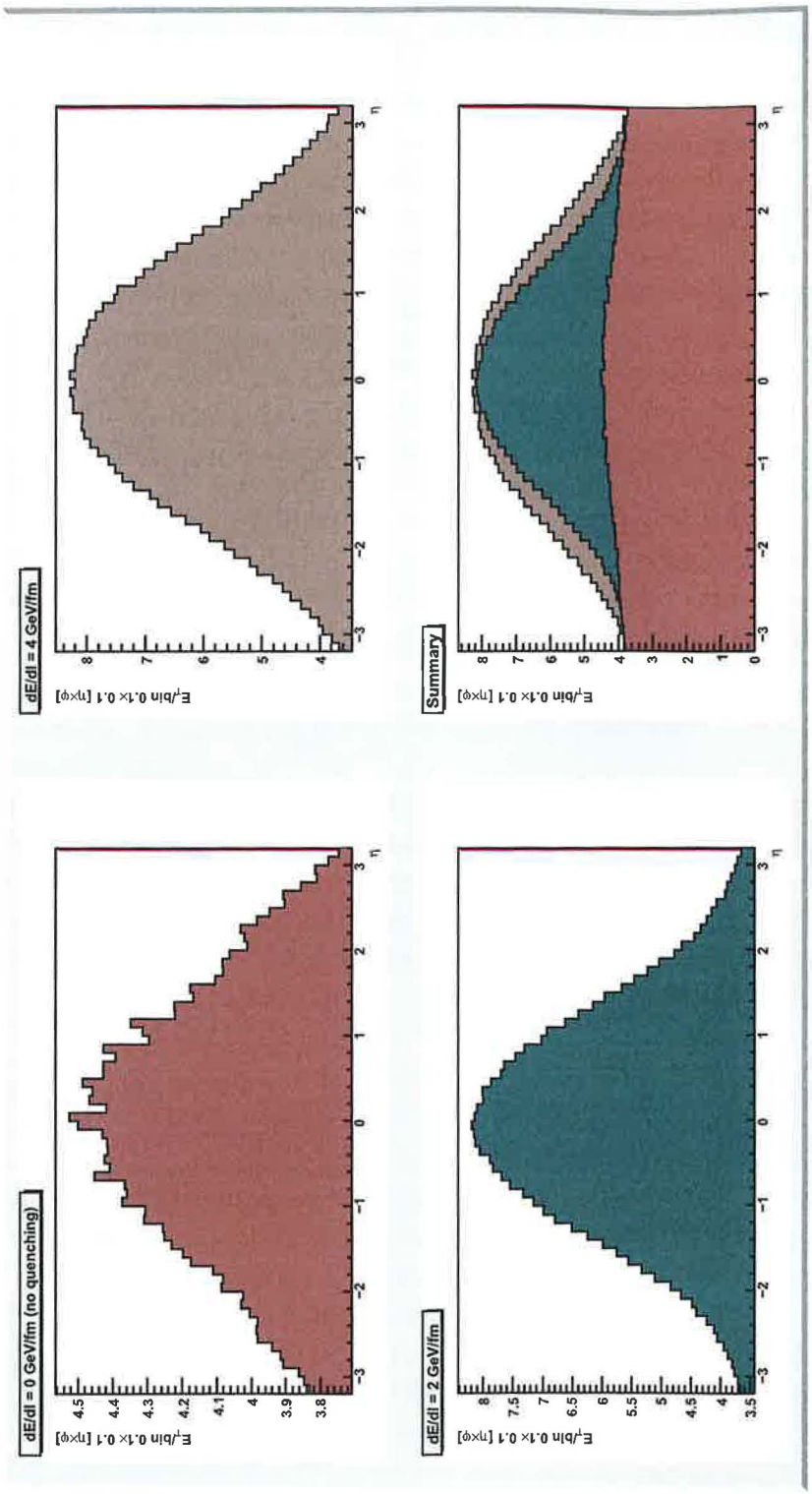

Figure 4.2: Dependence of the transverse energy E_{T} deposited into $\eta \times \phi = 0.1 \times 0.1$ bin on the pseudorapidity for three values of $\mathrm{d}E/\mathrm{d}l$.

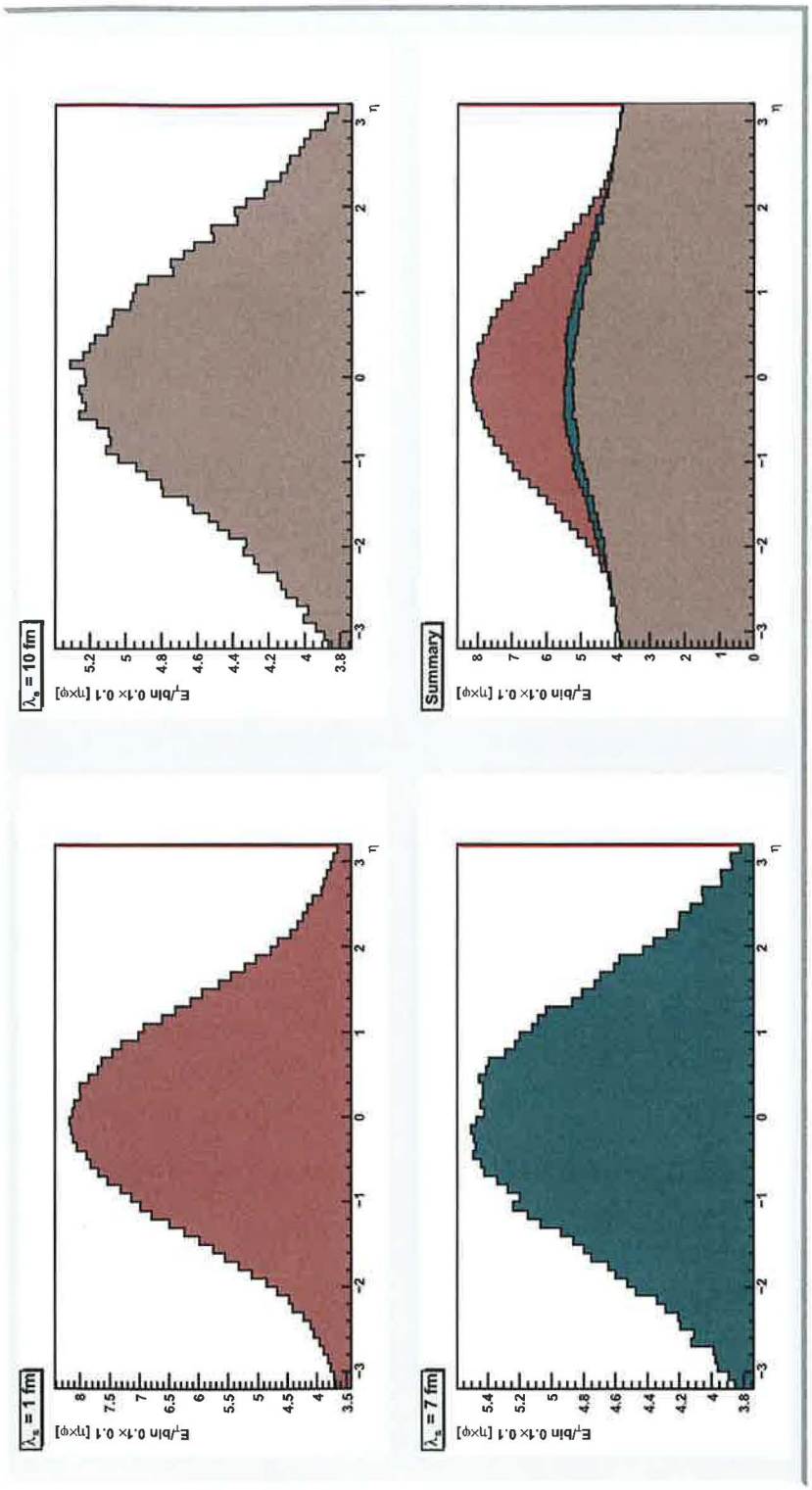

Figure 4.3: Dependence of the transverse energy E_{T} deposited into $\eta \times \phi = 0.1 \times 0.1$ bin on the pseudorapidity for three values of λ_s.

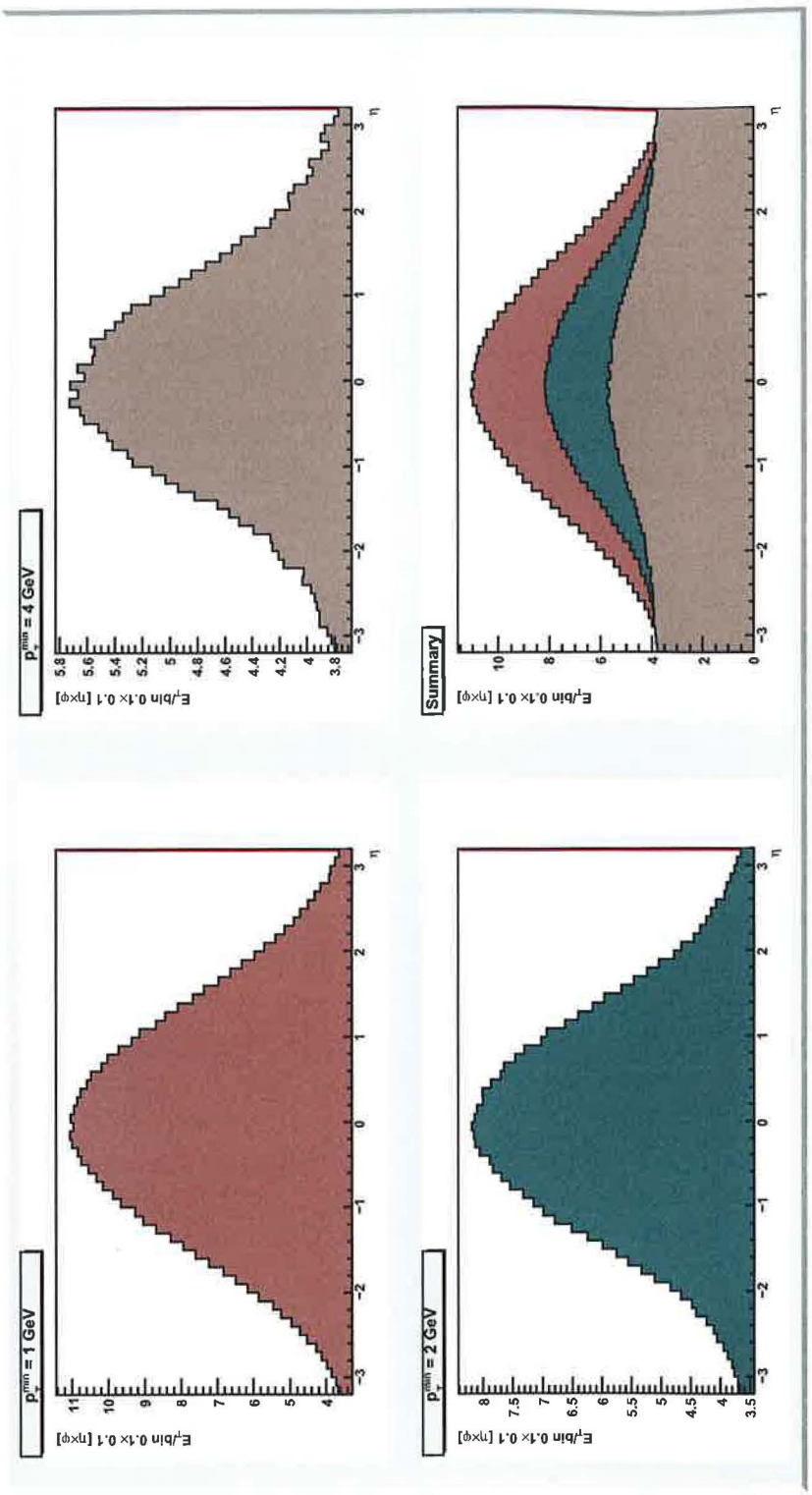

Figure 4.4: Dependence of the transverse energy E_{T} deposited into $\eta \times \phi = 0.1 \times 0.1$ bin on the pseudorapidity for three values of $p_{\mathrm{T}}^{\mathrm{min}}$.

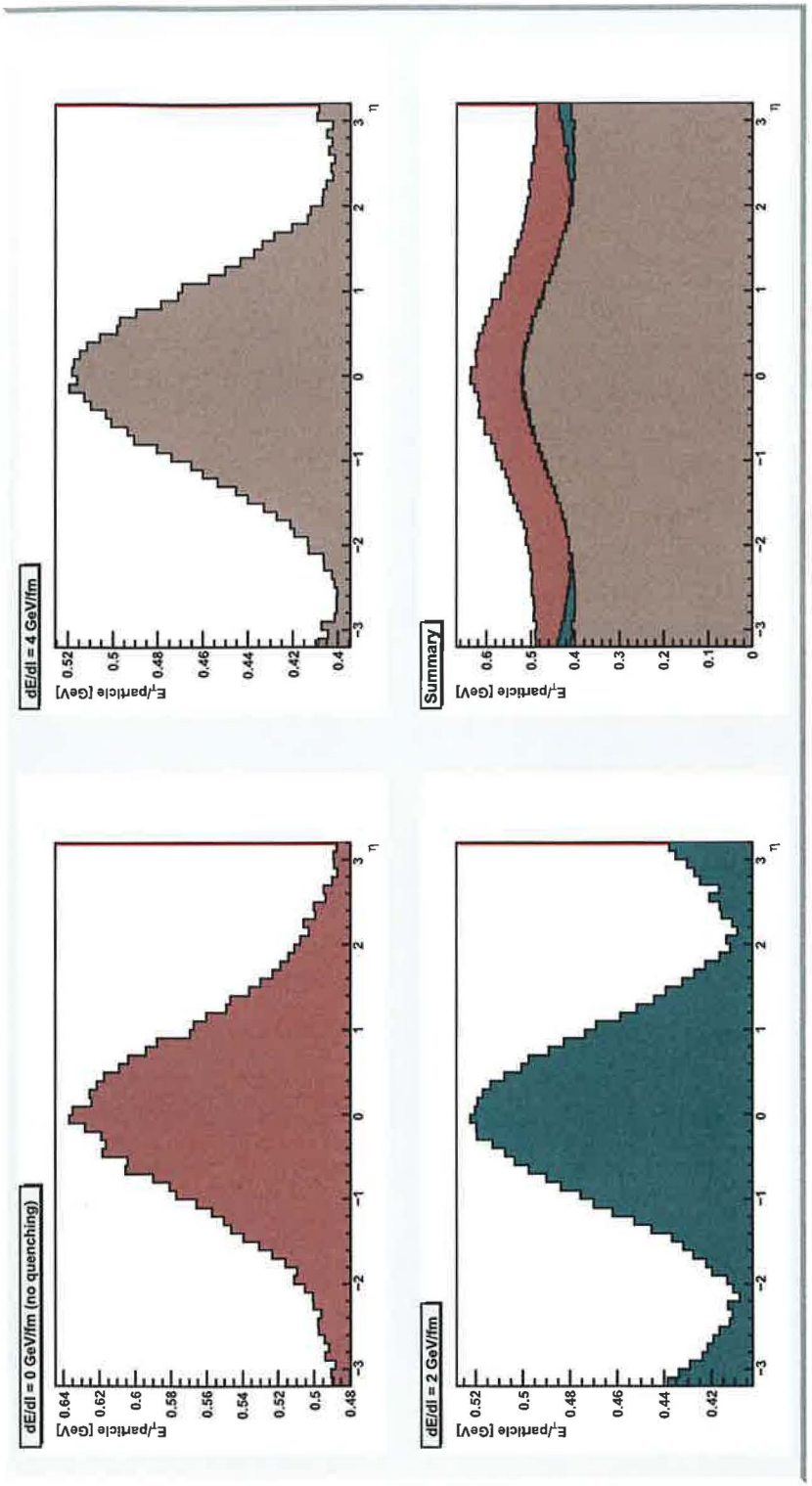

Figure 4.5: Dependence of mean transverse energy per particle for three values of $\mathrm{d}E/\mathrm{d}l$.

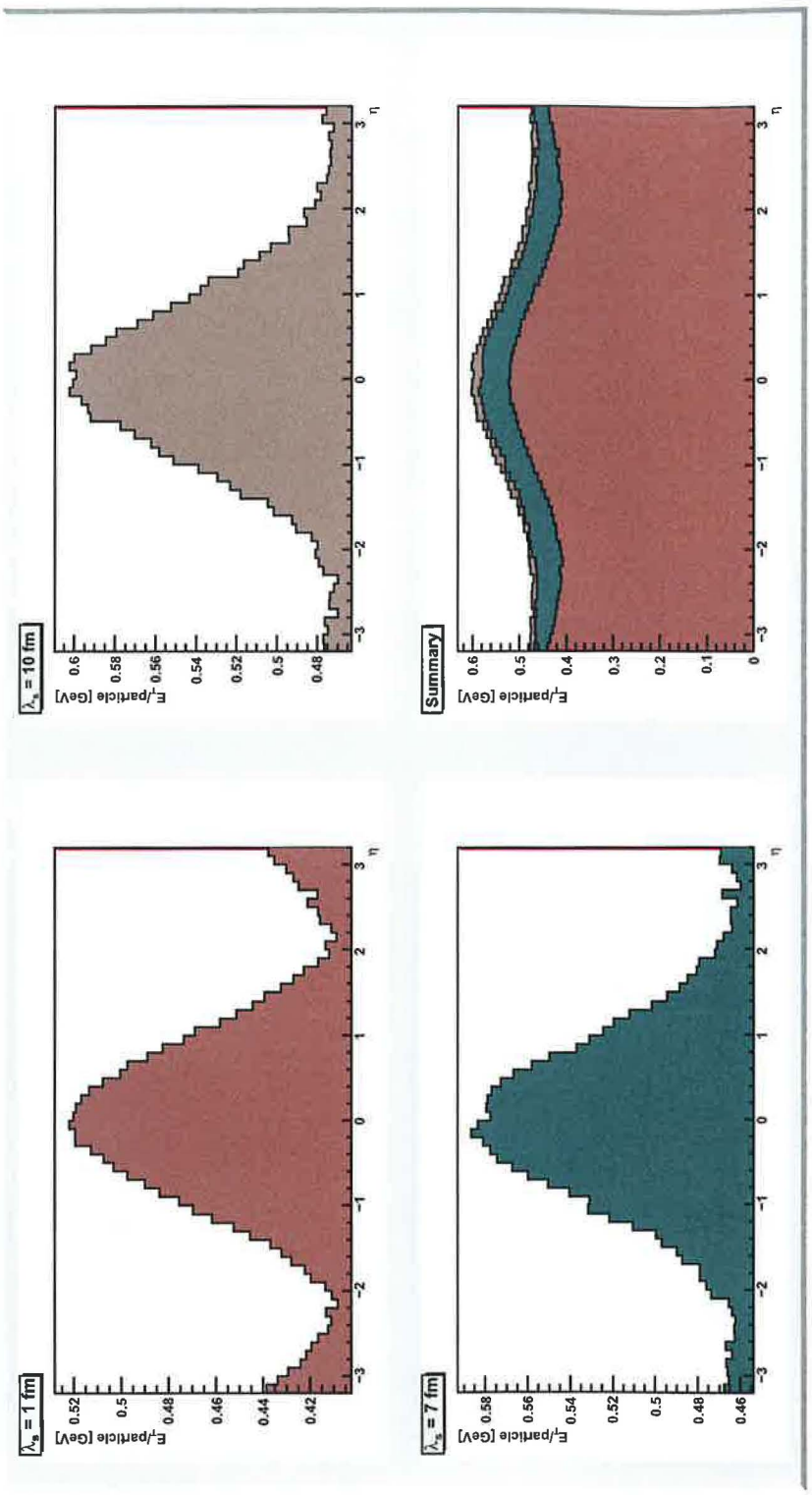

Figure 4.6: Dependence of mean transverse energy per particle for three values of λ_s.

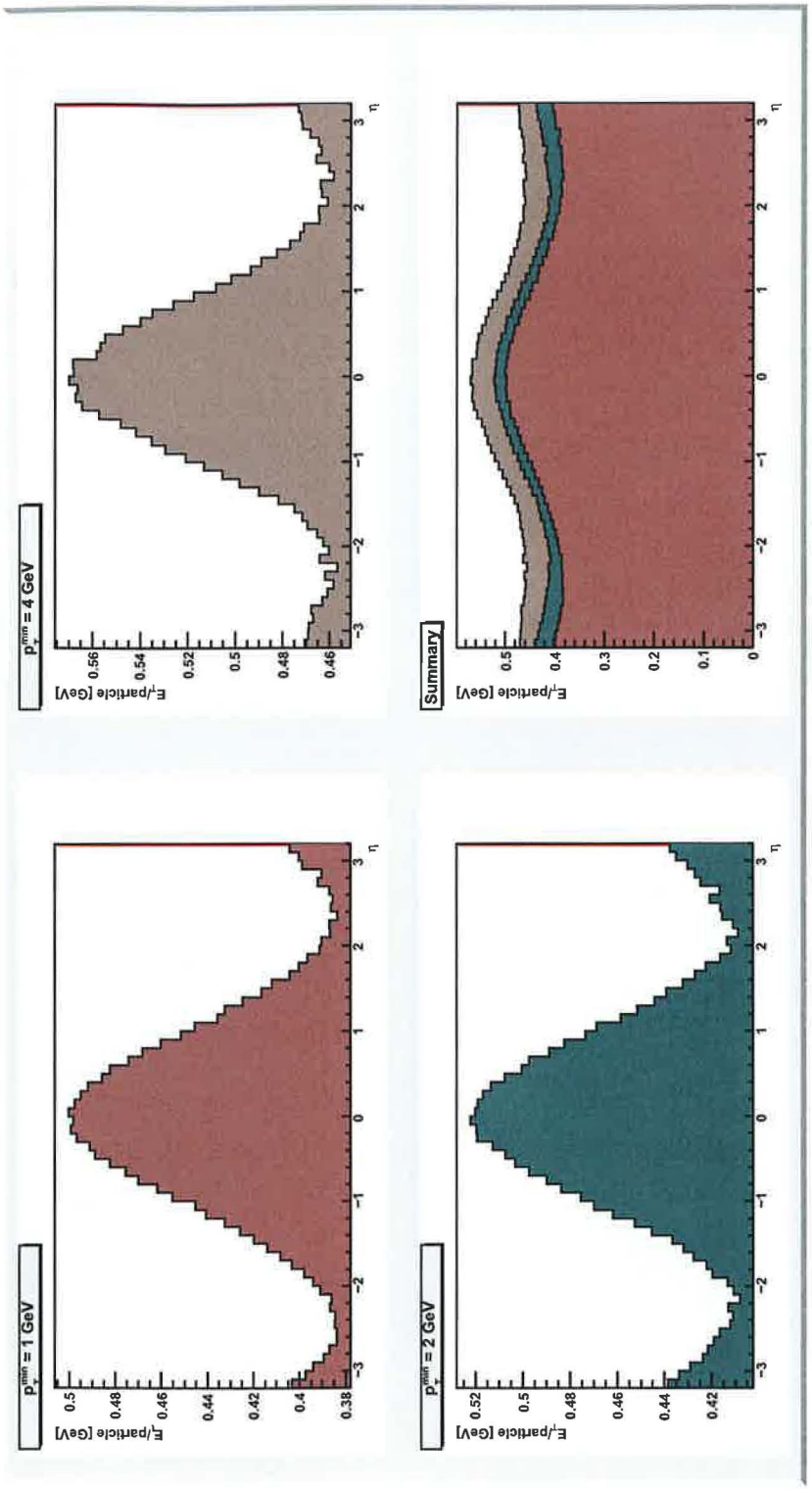

Figure 4.7: Dependence of mean transverse energy per particle for three values of $p_{\mathrm{T}}^{\mathrm{min}}$.

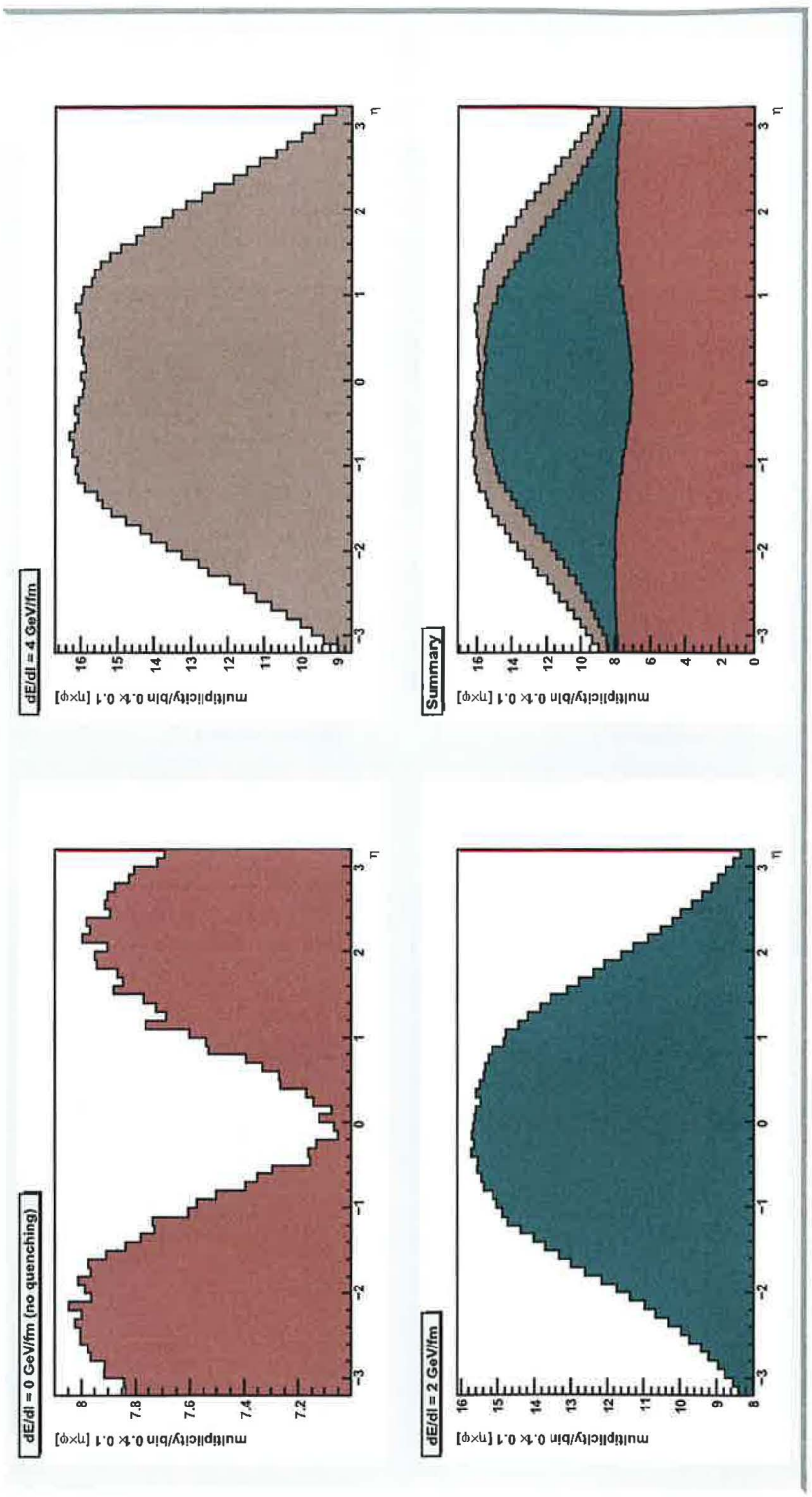

Figure 4.8: Dependence of multiplicity (into one bin) on the pseudorapidity for three values of $\mathrm{d}E/\mathrm{d}l$.

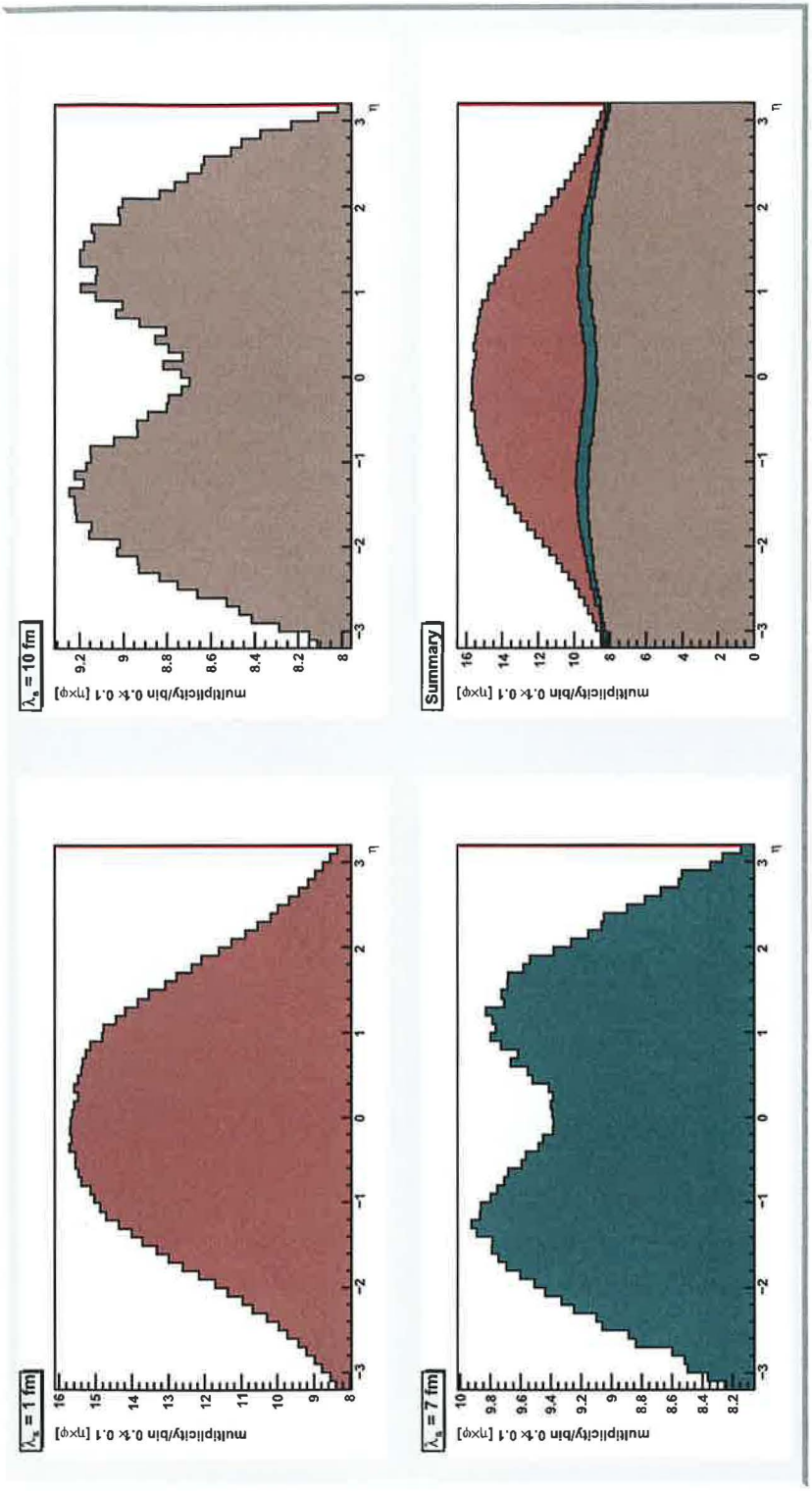

Figure 4.9: Dependence of multiplicity (into one bin) on the pseudorapidity for three values of λ_s.

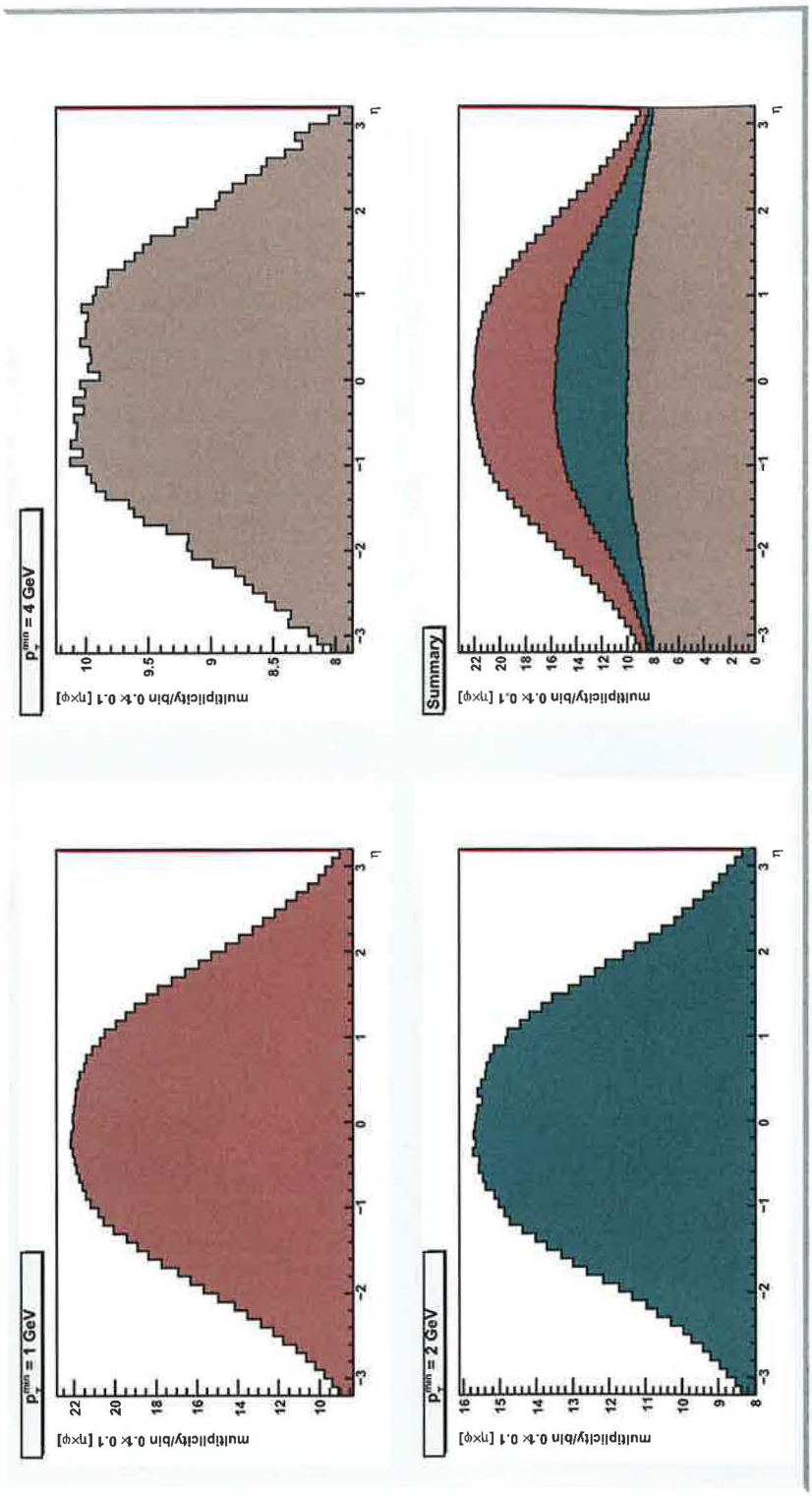

Figure 4.10: Dependence of multiplicity (into one bin) on the pseudorapidity for three values of $p_{\mathrm{T}}^{\mathrm{min}}$.

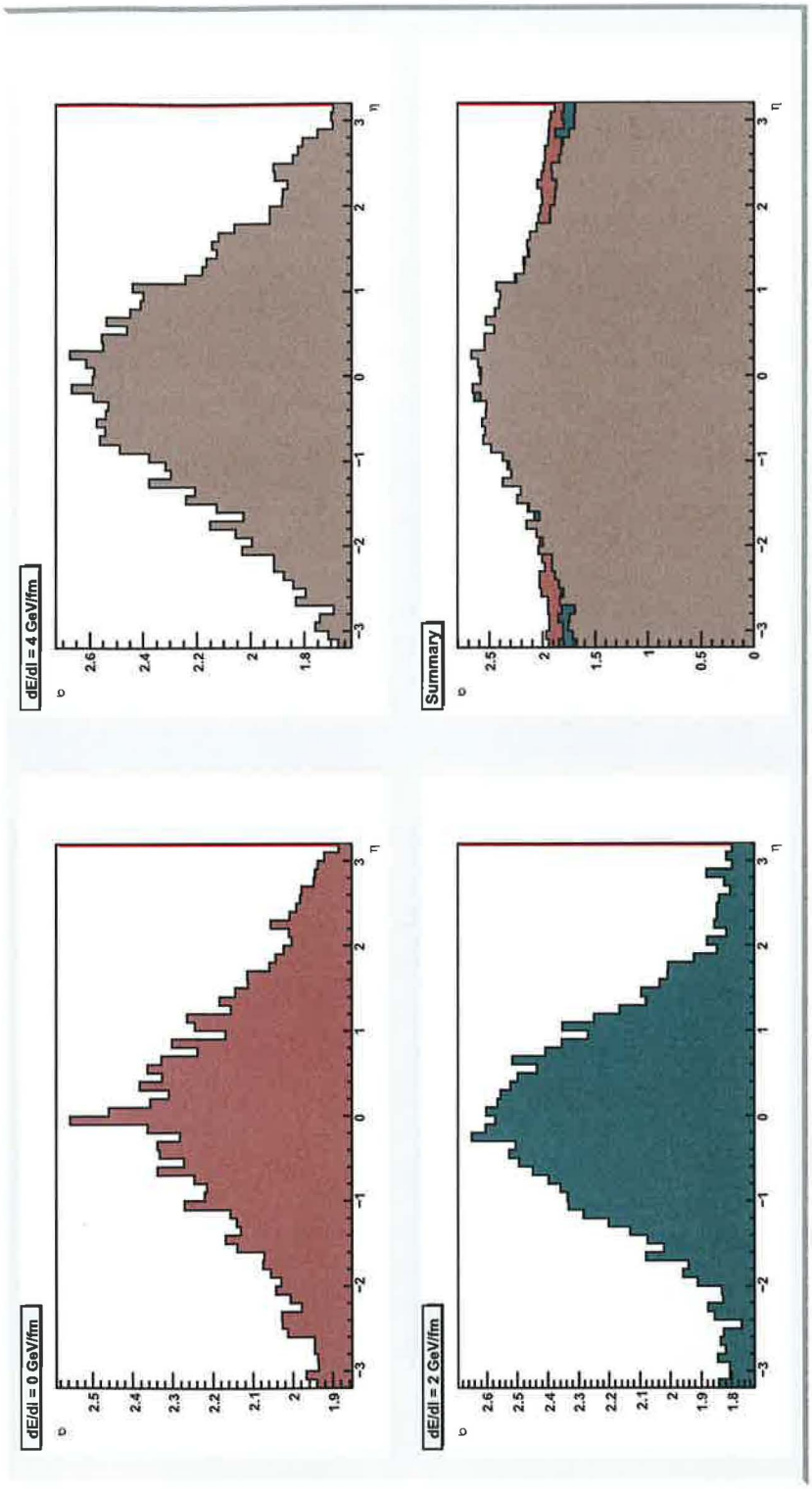

Figure 4.11: Dependence of standard deviation σ on the pseudorapidity for three values of $\mathrm{d}E/\mathrm{d}l$.

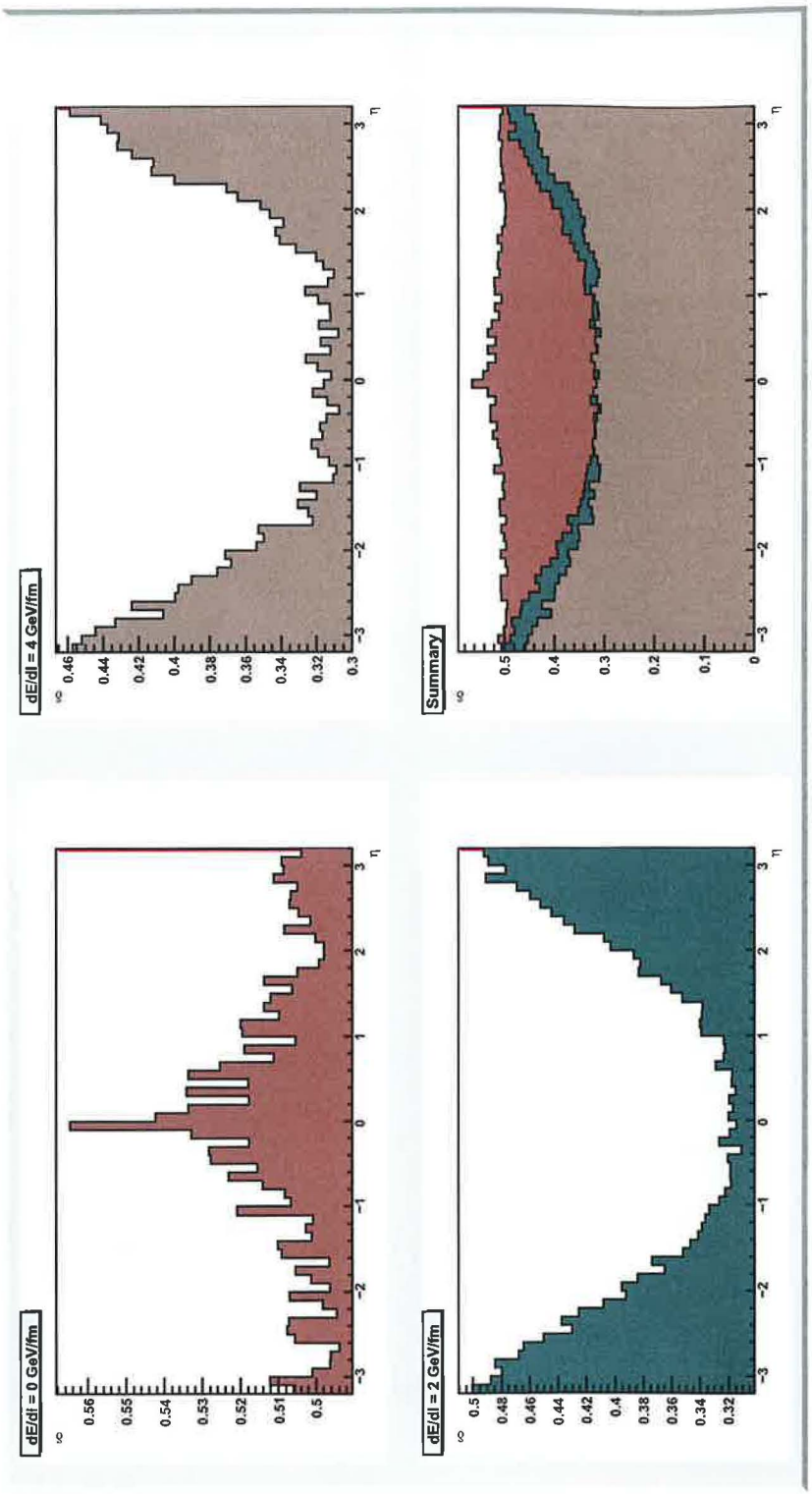

Figure 4.12: Dependence of relative standard deviation σ on the pseudorapidity for three values of $\mathrm{d}E/\mathrm{d}l$.

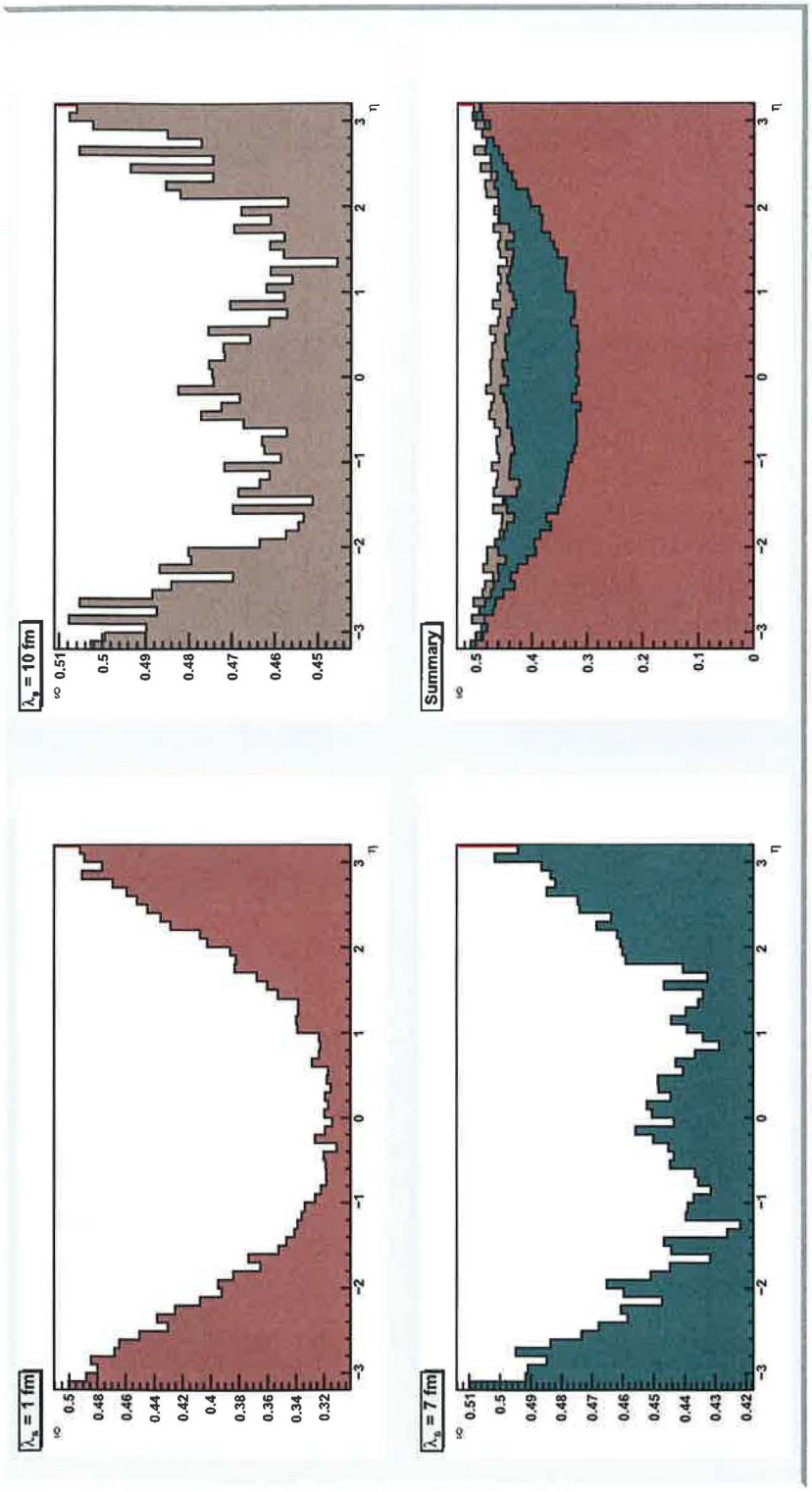

Figure 4.13: Dependence of relative standard deviation σ on the pseudorapidity for three values of λ_s.

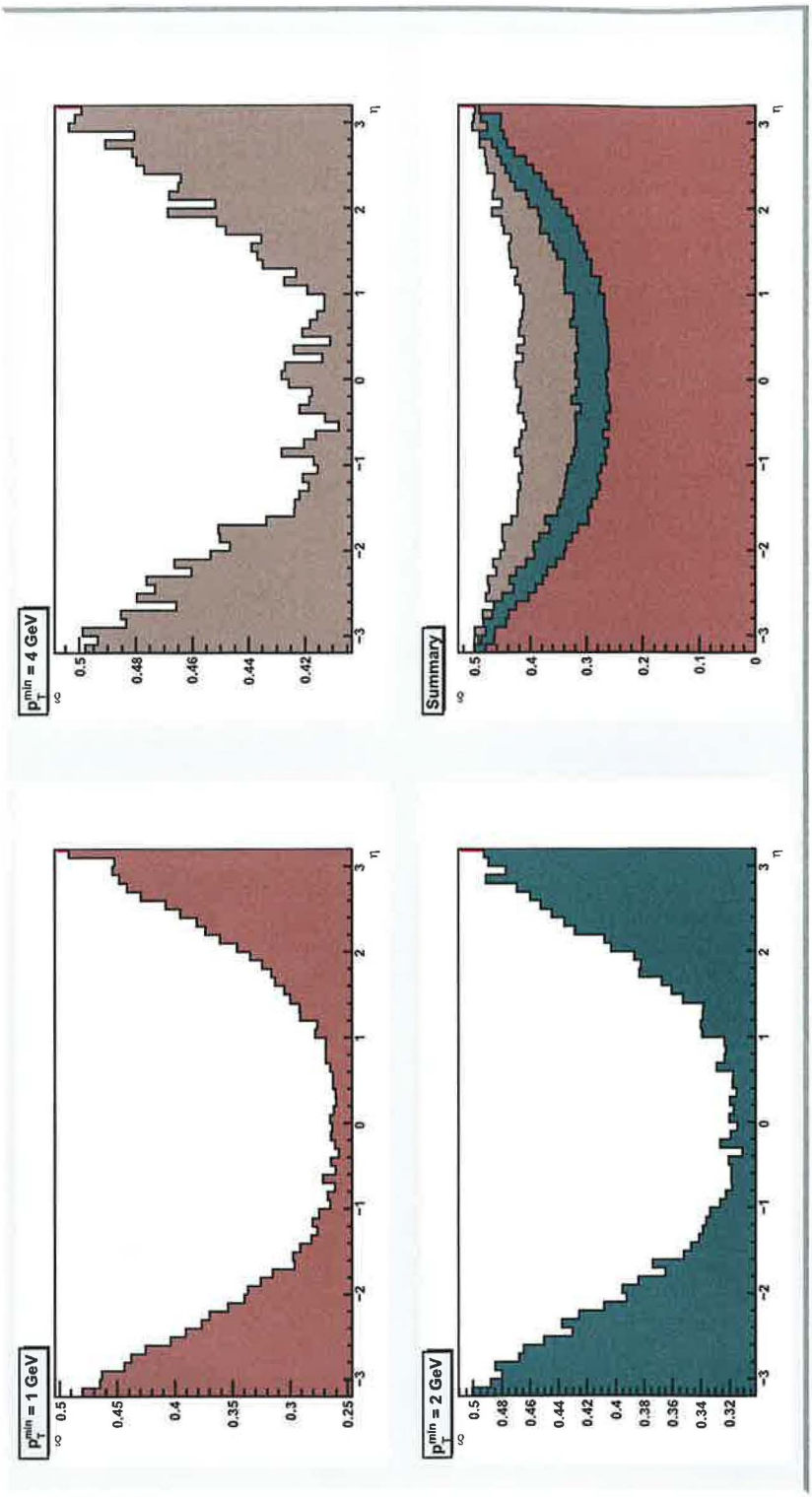

Figure 4.14: Dependence of relative standard deviation σ on the pseudorapidity for three values of $p_{\mathrm{T}}^{\mathrm{min}}$.

Chapter 5

PYQUEN

PYQUEN is Monte Carlo program written in Fortran 77 programming language by I. P. Lokhtin et al. to simulate jet quenching in heavy-ion collisions [30]. As compared with HIJING, PYQUEN does not generate the complete event, it "only" modifies Pythia generated jets as going through quark gluon-plasma. This is consistent with widely used approach where PYTHIA jets are embedded into HIJING event [31]. In PYQUEN, quark-gluon plasma is treated as continuum with initial conditions settled by user and evolving in time according to Bjorken model [14]. We will now describe in detail, how program works.

5.1 The main program

The main program has to be written by user. First the parameters of PYQUEN have to be set:

- beam properties: energy, nuclei mass number (`A`), impact parameter – fixed (`ifb = 0`, `bfix = b` [fm]) or minimum bias centrality with Glauber geometry (`ifb > 0`)
- properties of energy loss: type of energy loss (collisional + radiative, radiative, collisional, none), angular distribution of emitted gluons,
- QGP initial properties: temperature T_0, time of QGP formation τ_0, number of active quark flavours N_f
- Pythia properties
- number of events to be generated

Then the loop over events follows. In this loop:

1. partonic event is generated: `call pyevnt`
2. PYQUEN program is called to modify generated PYTHIA event `call pyquen(A, ifb, bfix)`. See below

3. hadronization routine is called: `call pyexec`

4. unstable particles and partons are removed: `call pyedit(2)`

5. generated event is saved

In procedure `pyquen` first the initialization and check of the set parameters is done. Then two arrays are tabulated – these arrays are later used for interpolation of nuclear thickness function $T_A(\mathbf{b})$ and nuclear overlap function $T_{AB}(\mathbf{b})$. After that, if impact parameter isn't fixed, it is randomly generated according to probability distribution

$$F(\mathbf{b}) = T_{AB}(\mathbf{b}).b.[1 - \exp\left(T_{AB}(\mathbf{b})\sigma_{in}\right)] \tag{5.1}$$

Then the medium properties are calculated by call of procedure `plinit`. According to Bjorken model, medium is treated as a boost-invariant longitudinally expanding quark-gluon fluid. For temperature $T > T_c$ the energy density, temperature and density are evolving in time as

$$\epsilon(\tau)\tau^{4/3} = \epsilon_0\tau_0^{4/3}, \qquad T(\tau)\tau^{1/3} = T_0\tau_0^{1/3}, \qquad \rho(\tau)\tau = \rho_0(\tau)\tau_0 \tag{5.2}$$

After that, the procedure `plevnt` is called. This procedure contains the most important part of physics since it manages the parton rescatering and energy loss. We describe this procedure in next section.

5.2 Parton rescattering and energy loss

First the vertex of jet production is generated according to the distribution

$$\frac{\mathrm{d}N^{\mathrm{jet}}}{\mathrm{d}\psi\,\mathrm{d}r}(b) = \frac{T_A(r_1)T_A(r_2)}{T_{AA}(b)} \tag{5.3}$$

where $r_{1,2}$ are the distances between the nucleus centres and jet production vertex – see figure 5.1. It can be shown that

$$r_{1,2} = \sqrt{r^2 + \frac{b^2}{4} \pm rb\cos\psi} \tag{5.4}$$

After that, loop over particles generated by Pythia is done

1. only partons with $p_{\mathrm{T}} > 3$ GeV and $|\eta| < 7$ are then taken into account.

2. colour factor is set: 1 for gluons, 4/9 for quarks

3. the proper time of parton leaving the dense zone (QGP) is calculated

$$\begin{aligned} \tau_{\mathrm{L}} \;=\; & min\{\sqrt{R_A^2 - r_1^2\sin\varphi^2} - r_1\cos\varphi, \\ & \sqrt{R_A^2 - r_2^2\sin\left(\varphi - \varphi_0\right)^2} - r_2\cos\left(\varphi - \varphi_0\right)\} \end{aligned} \tag{5.5}$$

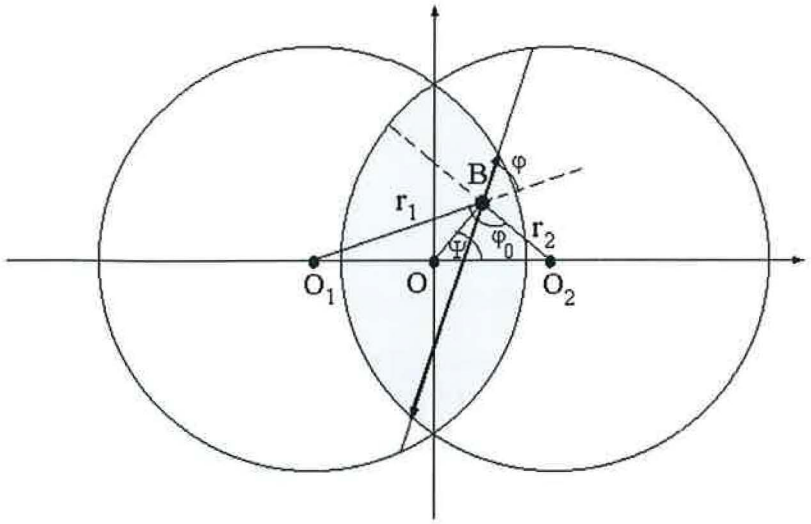

Figure 5.1: The geometry of jet quenching [32]

where φ_0 is the angle between vectors $\mathbf{r}_1$ and $\mathbf{r}_2$

$$\varphi_0 = \arccos \frac{r^2 - b^2/4}{r_1 r_2} \tag{5.6}$$

If τ_L is smaller than τ_0, i. e. if parton leaves the dense zone before QGP formation, the loop is left.

4. displacement l_i between i-th and $(i+1)$-th scattering is generated according to probability

$$\frac{\mathrm{d}P}{\mathrm{d}l_i} = \lambda^{-1}(\tau_{i+1}) \exp\left(-\int_0^{l_i} \lambda^{-1}(\tau_i + s)\,\mathrm{d}s\right) \tag{5.7}$$

If now velocity is smaller than 0.3, temperature is bellow T_c loop is left

5. parton energy is reduced by call of routine `pljetr`. Both collisional and radiative energy loss are considered for each scattering (or one of them or none of them).

$$\Delta E_{\mathrm{tot},i} = \Delta E_{\mathrm{col},i} + \Delta E_{\mathrm{rad},i} \tag{5.8}$$

The collisional energy loss is calculated in the high-momentum transfer approximation

$$\Delta E_{\mathrm{col},i} = \frac{t_i}{2m_0} \tag{5.9}$$

and radiative energy loss is calculated via BDMS framework. Then $\Delta E_{\mathrm{rad},i} = \omega_i$ where ω_i is energy of the radiated gluon which is generated according to (see also section 3.1)

$$\left.\frac{\mathrm{d}I}{\mathrm{d}\omega}\right|_{m_{\mathrm{q}}=0} = \frac{2\alpha_s(\mu_D^2)\lambda C_R}{\pi L\omega}\left[1-y+\frac{y^2}{2}\right]\ln\left|\cos\left(\omega_1\tau_1\right)\right| \tag{5.10}$$

$$\left.\frac{\mathrm{d}I}{\mathrm{d}\omega}\right|_{m_{\mathrm{q}}\neq 0} = \frac{1}{(1+(\beta\omega)^{3/2})^2}\left.\frac{\mathrm{d}I}{\mathrm{d}\omega}\right|_{m_{\mathrm{q}}=0} \tag{5.11}$$

In the `pljetr` also the momentum kick due to elastic scattering is calculated

6. The angle of the emitted gluon is generated – user can set type of angular distribution: small angular distribution, wide angular distribution or collinear distribution. Emitted gluons are added to the parton list.

5.3 Simulations

We used PYQUEN to simulate jet modifications in heavy ion collisions as will be performed at LHC : PbPb collisions at $\sqrt{s_{\mathrm{NN}}} = 5500$ GeV. The impact parameter was fixed to $b = 2$ fm. As we have noticed, PYQUEN does not generate full event, so the value of impact parameter influences only the size of the dense zone and consequently the length of the distance parton has to traverse through medium. Pythia was called to generate proton-proton collisions with initial hard sub-process cutoff $p_{\mathrm{T}} > 50$ GeV. The data were simulated with three types of energy loss: no energy loss, only radiative energy loss and both radiative and collisional energy loss.

We extracted two basic quantities from the simulated events. First is the p_{T} spectrum of the events which is shown in figure 5.2. As we can see, the results are reasonable: spectrum is hardest for events without energy loss for high p_{T}, if we turn on radiative energy loss, the significant softening of the spectrum arose. With both radiative and collisional energy loss spectrum is the softest.

Another interesting observable is the azimuthal correlations. These correlations were obtained according to following algorithm: first the hardest (leading) parton in the event was found, then its azimuthal angle was set to zero and the azimuthal angles of the remaining partons were calculated relative to the hardest parton. Then the transverse energy was deposited into the according direction. As we know, jets are produced with opposite directions in the transverse plane so the double peak distribution is expected. Histograms with our correlations are in figure 5.3. As we can see, the highest deposited transverse energy is for unquenched events both in near side and away side peak. However very interesting is, that deposited transverse energy for only radiative energy loss is smaller than for radiative + collisional energy loss in the away side peak – this is clearly exhibited in figure 5.4. The origin of this phenomenon is not completely clear, the explanation requires more refined analyses than we are nowadays able to do.

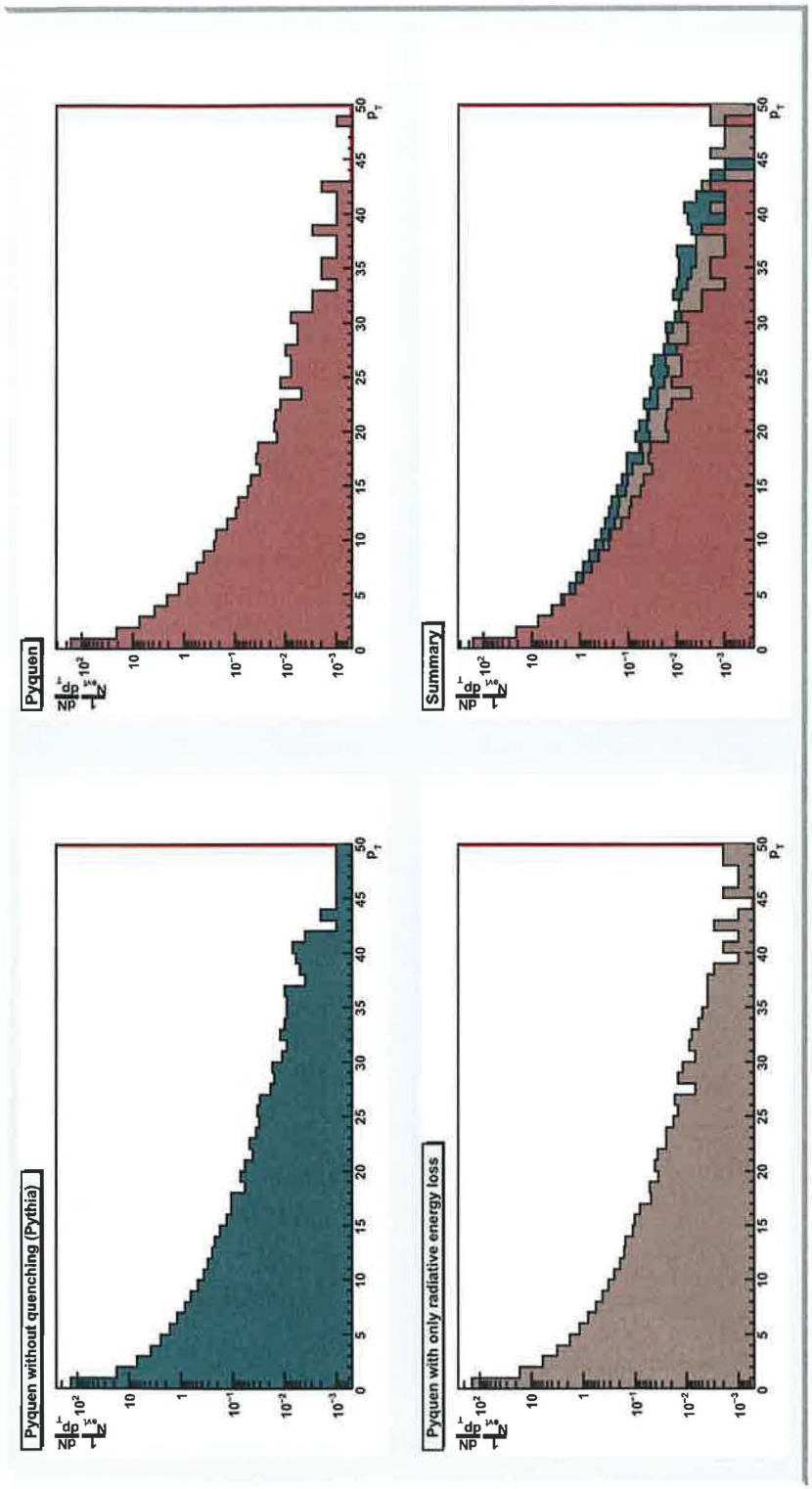

Figure 5.2: p_{T}-spectrum for three types of energy loss

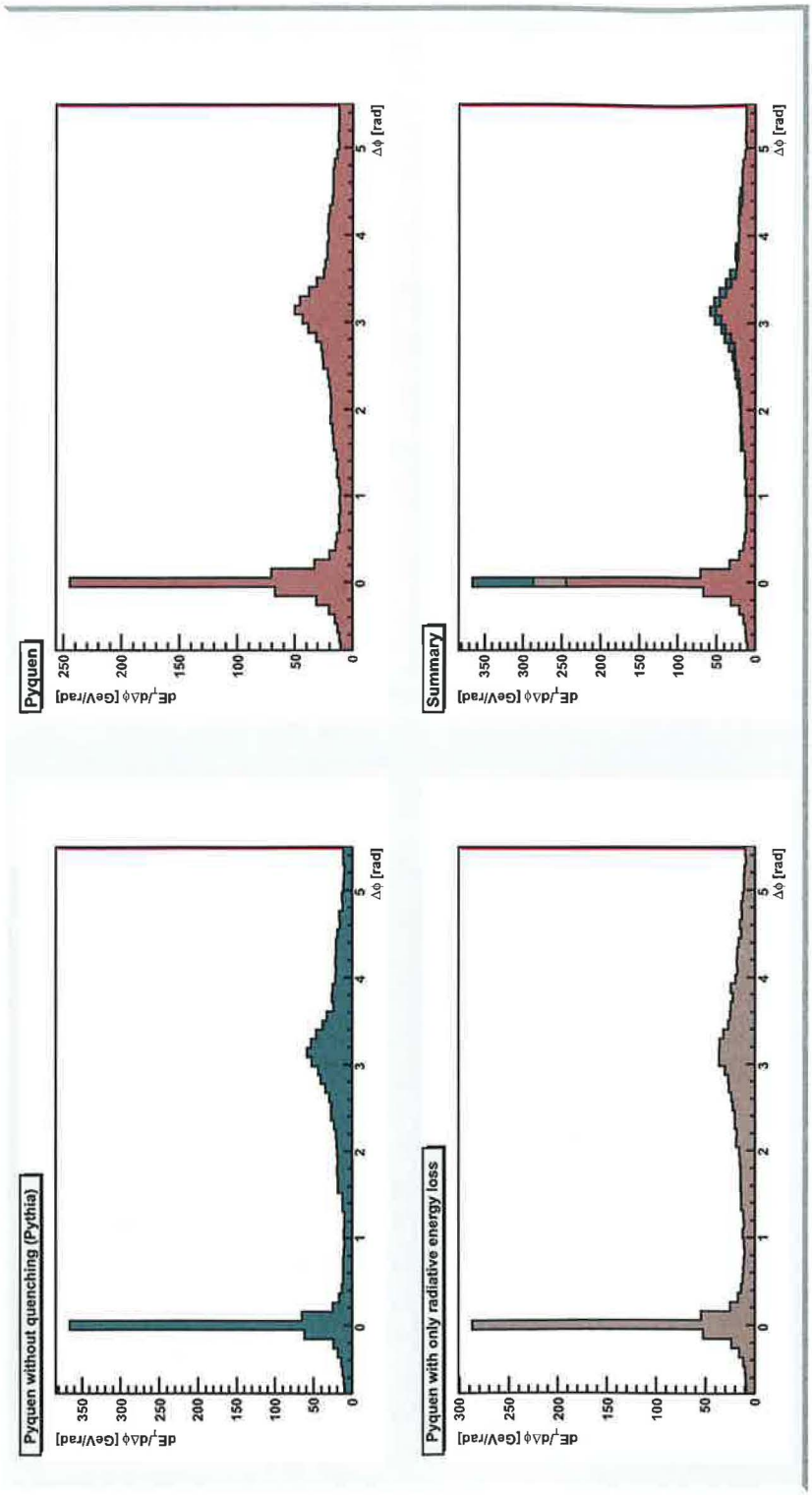

Figure 5.3: Azimuthal correlations of transverse energy for three types of energy loss.

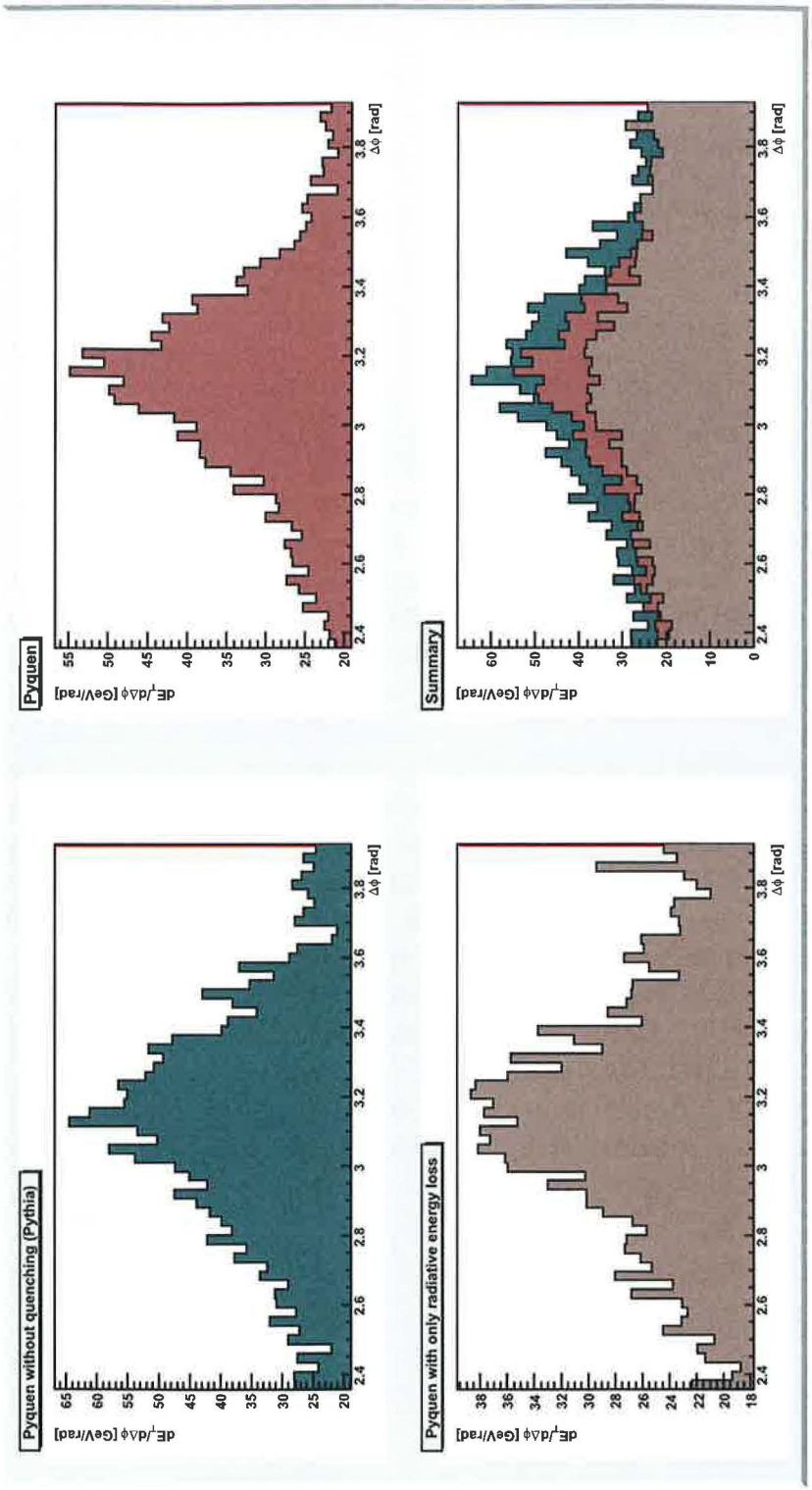

Figure 5.4: Azimuthal correlations of transverse energy for three types of energy loss – detail of away-side peak

Chapter 6

Conclusion

Two programs, HIJING resp. PYQUEN, used for simulations of heavy ion collisions and jet quenching were analysed. In the case of HIJING, the important part of the source code was read, mainly that part managing hard part of the heavy ion collision with special emphasis placed on procedure `QUENCH`. The description of this part of program is in sections 4.1-4.3. Four free parameters of jet quenching model were discussed. From the description of the quenching procedure, we can see that model for jet quenching in HIJING is very simple and rather schematic.

Then we used HIJING for simulations of PbPb collisions as will be run at LHC and by variation of three of four parameters, we analysed how jet quenching as implemented in HIJING changes various physical characteristics of the event. The results of this simulations are in figures 4.2-4.14. As we can see, the fact whether jet quenching is turned on or of significantly changes behaviour of the program. The conclusion of this part of work is, that *usage of HIJING program with quenching procedure turned on should be carefully considered since it produces significant changes in physical characteristics.*

The source code of the second of studied programs, PYQUEN, was also read. The description of the program is in chapter 5. Jet quenching in PYQUEN is treated more precisely and the model is much more physical than model implemented in HIJING. On the other hand, PYQUEN does not generate complete event, it only modifies events generated by Pythia, so one is unable to obtain many physical quantities only with PYQUEN.

Bibliography

[1] J. Chýla, Quarks, partons and Quantum Chromodynamics, http://www-hep2.fzu.cz/ chyla/lectures/text.pdf

[2] W. Greiner, S.Schramm, E.Stein, Quantum Chromodynamics, Springer Verlag, Berlin, 1. Edition (2001)

[3] G. Sterman et al., Handbook of perturbative QCD, Rev. Mod. Phys. 67, 157 - 248 (1995)

[4] Particle Data Group, Particle Physics Booklet, 2002, http://pdg.lbl.gov

[5] B. Andersson et al., Parton Fragmentation and String Dynamics, PhysRep 97 31 - 145 (1983)

[6] S. Hands, The Phase Diagram of QCD, arXiv:physics/0105022 (2001)

[7] http://www-cdf.fnal.gov/experiment/events/events.html

[8] M. E. Peskin, D. V. Schroeder, An Introduction to Quantum Field Theory, Perseus Books, Cambridge (1995)

[9] L. McLerran, The physics of the quark-gluon plasma, Rev. Mod. Phys. 58, 1021 - 1064 (1986)

[10] C. O. E. Jorgensen, Charged Particle Production in Au+Au Collisions at $\sqrt{s_{NN}} =$ 130 GeV, Master thesis, University of Copenhagen (2001)

[11] P. Braun-Munzinger, D. Magestro, K. Redlich, J. Stachel, Hadron production in Au-Au collisions at RHIC, Phys.Lett.B518 (2001)

[12] A. Bazavov et al., Equation of state and QCD transition at finite temperature, Phys. Rev. D 80, 014504 (2009)

[13] K. Rajagopal, The Phases of QCD in Heavy Ion Collisions and Compact Stars, Acta Phys.Polon. B31 (2000)

[14] J. D. Bjorken, Highly relativstic nucleus-nucleus collisions: The central rapidity region, Phys.Rev.D27 140 (1983)

[15] K. Geiger, High Density QCD and Entropy Production at Heavy Ion Colliders, arXiv:hep-ph/9409219 (1994)

[16] Cheuk-Yin Wong, Introduction to High-Energy Heavy-Ion Collisions, World Scientifc (1994)

[17] G. Torrieri, Phenomenology of strangeness enhancement in heavy-ion collisions, J. Phys. G: Nucl. Part. Phys. 36 064007 (2009)

[18] C. A. Ogilvie, Review of Nuclear Reactions at the AGS, Nuclear Physics A698 (2002)

[19] K. Yagi, T. Hatsuda, Y. Miake, Quark-Gluon plasma: from big bang to little bang, Cambridge University Press (2005)

[20] NA50 Collaboration, Evidence for deconfinement of quarks and gluons from the J/ψ suppression pattern measured in Pb-Pb collisions at the CERN-SPS, Phys. Lett. B 477, 28 (2000)

[21] L.V. Bravina et al., Elliptic flow at RHIC: Where and when was it formed?, Phys.Lett. B631 109-117 (2005)

[22] A. Taranenko, PHENIX studies of the scaling properties of elliptic flow at RHIC, J. Phys. G: Nucl. Part. Phys. 34 (2007)

[23] D. d'Enterria, Jet quenching, arXiv:0902.2011 (2009)

[24] S. Peigne, A.V. Smilga, Energy losses in a hot plasma revisited, arXiv:0810.5702v1 (2008)

[25] B. I. Abelev et al. [STAR Collaboration]: Energy dependence of $\pi^{\pm}$, p and $\bar{\text{p}}$ transverse momentum spectra for Au+Au collisions at $\sqrt{s_{NN}} = 62.4$ and 200 GeV, arXiv:nucl-ex/0703040 (2007)

[26] J. Adams et al. [STAR Collaboration]: Evidence from d+Au measurements for final-state suppression of high p_T hadrons in Au+Au collisions at RHIC, arXiv:nucl-ex/0306024 (2003)

[27] X. N. Wang, M. Gyulassy, HIJING: A Monte Carlo model for multiple jet production in pp, pA and AA collisions, Phys. Rev. D 44, 3501 - 3516 (1991)

[28] http://www-nsdth.lbl.gov/~xnwang/hijing/doc.html

[29] X.-N. Wang, pQCD based approach to parton production and equilibration in high-energy nuclear collisions, Phys.Rept. 280 (1997)

[30] I.P. Lokhtin, A.M. Snigirev, A model of jet quenching in ultrarelativistic heavy ion collisions and high-pt hadron spectra at RHIC, Eur. Phys. J C46 (2006)

[31] J. Dolejší, M. Rybář, M. Spousta, Private discussions

[32] I.P. Lokhtin, A.M. Snigirev, Nuclear geometry of jet quenching, Eur. Phys. J C16 (2000)

Appendix A

Parton model

Parton model was developed in the late 60's to explain experimental results obtained from electron proton scattering [1, 8]. The basic assumption of parton model is, that protons (or generally hadrons) are composed of loosely bound partons. Thus if one imagine high energy collision of electron (with initial (final) momentum k (k')) and proton with initial momentum P in the center of mass frame, partons have lightlike momentum p almost collinear with proton. In other words, at sufficiently high energies, we can neglect Fermi motion of parton within proton. Thus we can write

$$p = \xi P \tag{A.1}$$

where ξ is a number between 0 and 1. It can be shown that this fraction coincide with relativistically invariant variable x (also called Bjorken-x) which can be obtained from experiment if final electron's momentum is measured:

$$x = \frac{Q^2}{2P.q} \tag{A.2}$$

where $q = k - k'$ is the momentum transfer, and Q^2 is the invariant momentum transfer $q^2 = -Q^2$. We will thus write x instead of ξ.

Both electron and quark are electrically charged fermions thus their cross section is calculable in QED. If we now multiply this cross section by the probability that proton contains a certain constituent with a certain momentum fraction x (expressed as the function $f_f(x)$) and integrate over x, we obtain the electron-proton cross section

$$\sigma\left(e^-(k)p(P) \to e^-(k') + X\right) = \int_0^1 \sum_f f_f(x)\sigma\left(e^-(k)q_f(xP) \to e^-(k') + q_f(p')\right) \tag{A.3}$$

where $f_f(x)$ is usually called parton distribution function (PDF). However, since the PDF are governed by soft processes, they cannot be determined by pQCD and thus they have to be extracted from experiment. It should be also noted, that parton distribution functions depend on the momentum squared Q^2. But the dependence is weak and can be neglected in the first order calculations.

Since the parton distribution functions are the probabilities of finding partons inside the hadrons, they must be normalized in a way that reflects the quantum numbers of the hadron. For example proton is composed of two u and one d valence quarks plus some admixture of quark-antiquark pairs and gluons. Thus it should hold

$$\int_0^1 \mathrm{d}x[f_u(x) - f_{\bar{u}}(x)] = 2, \qquad \int_0^1 \mathrm{d}x[f_d(x) - f_{\bar{d}}(x)] = 1 \tag{A.4}$$

Since the total amount of momentum carried by partons must be equal to the momentum of the hadron. This implies

$$\int_0^1 \mathrm{d}x\, x[f_u(x) + f_d(x) + f_{\bar{u}}(x) + f_{\bar{d}}(x)] = 1 \tag{A.5}$$

Appendix B

The Lowest order QCD matrix elements

Process	$\overline{\lvert\mathcal{M}\rvert^2}$
$q_1q_2 \to q_1q_2$ $q_1\bar{q}_2 \to q_1\bar{q}_2$	$\left\{\frac{4}{9}\frac{s^2+u^2}{t}\right.$
$q_1q_2 \to q_1q_1$	$\frac{4}{9}\left(\frac{s^2+u^2}{t^2}\right)+\frac{4}{9}\left(\frac{s^2+t^2}{u^2}\right)-\frac{8}{27}\frac{s^2}{ut}$
$q_1\bar{q}_1 \to q_2\bar{q}_2$	$\frac{4}{9}\left(\frac{t^2+u^2}{s^2}\right)$
$q_1\bar{q}_1 \to q_1\bar{q}_1$	$\frac{4}{9}\left(\frac{s^2+u^2}{t^2}\right)+\frac{4}{9}\left(\frac{t^2+u^2}{s^2}\right)-\frac{8}{27}\frac{u^2}{ts}$
$q\bar{q} \to gg$	$\frac{32}{27}\left(\frac{u^2+t^2}{ut}\right)-\frac{3}{8}\left(\frac{u^2+t^2}{s^2}\right)$
$gg \to q\bar{q}$	$\frac{1}{6}\left(\frac{u^2+t^2}{ut}\right)^2-\frac{3}{8}\left(\frac{u^2+t^2}{s^2}\right)$
$qg \to qg$	$-\frac{4}{9}\left(\frac{u^2+s^2}{us}\right)+\frac{u^2+s^2}{t^2}$
$gg \to gg$	$\frac{9}{2}\left(3-\frac{ut}{s^2}-\frac{us}{t^2}-\frac{st}{u^2}\right)$

Table B.1: Table of the lowest order parton-parton martix elements squared